High-resolution physicochemical dataset of atmospheric aerosols over the Tibetan Plateau and its surroundings

Jianzhong Xu[1,2*], Xinghua Zhang[2,a*], Wenhui Zhao[2,3,b], Lixiang Zhai[2,3,c], Miao Zhong[2,3], Jinsen Shi[4], Junying Sun[5], Yanmei Liu[2,d], Conghui Xie[2,e], Yulong Tan[2,3], Kemei Li[2,3], Xinlei Ge[6], Qi Zhang[7], Shichang Kang[2,3,8]

[1]School of Oceanography, Shanghai Jiao Tong University, Shanghai 200030, China.

[2]State Key Laboratory of Cryospheric Sciences, Northwest Institute of Eco-Environment and Resources, Chinese Academy of Sciences, Lanzhou 730000, China

[3]University of Chinese Academy of Sciences, Beijing 100049, China

[4]Key Laboratory for Semi-Arid Climate Change of the Ministry of Education, College of Atmospheric Sciences, Lanzhou University, Lanzhou 730000, China

[5]Key Laboratory of Atmospheric Chemistry of CMA, Chinese Academy of Meteorological Sciences, Beijing 100081, China

[6]Jiangsu Key Laboratory of Atmospheric Environment Monitoring and Pollution Control, Collaborative Innovation Center of Atmospheric Environment and Equipment Technology, School of Environmental Science and Engineering, Nanjing University of Information Science and Technology, Nanjing 210044, China

[7]Department of Environmental Toxicology, University of California, Davis, CA 95616, USA

[8]CAS Center for Excellence in Tibetan Plateau Earth Sciences, Beijing 100085, China

[a]now at: College of Urban and Environmental Sciences, Northwest University, Xi'an 710127, China.

[b]now at: Institute of Geochemistry, Chinese Academy of Sciences, Guangzhou 510640, China.

[c]now at: College of Resources and Environmental Sciences, Gansu Agricultural University, Lanzhou 730000, China.

[d]now at: College of Resources and Environment, Aba Teachers University, Wenchuan 623002, China.

[e]now at: State Key Joint Laboratory of Environmental Simulation and Pollution Control, College of Environmental Sciences and Engineering, Peking University, Beijing 100871, China.

Correspondence to: Jianzhong Xu (jzxu78@sjtu.edu.cn; jzxu@lzb.ac.cn) and Xinghua Zhang (zhangxinghua@lzb.ac.cn)

Abstract

Atmospheric aerosol in the Tibetan Plateau (TP) and its surroundings has ~~received widely~~ attracted significant scientific ~~concern~~interest in recent decades ~~owing~~due to its ~~significant~~notable impacts on ~~regional~~regionally climatic and cryospheric changes, ecological and environmental securities, and the hydrological cycle. However, our understanding on the atmospheric aerosol in this remote region is highly limited by the ~~scarcely~~scarcity of available dataset ~~due~~, owing to the extremely harsh natural conditions. This ~~condition~~challenge has been ~~improved~~mitigated in recent decades by ~~constructing a few stable~~establishing field observatories at typical sites ~~on~~within the TP and its surroundings. A continuous project ~~was carried out since~~ initiated in 2015 aims to ~~investigate~~explore the properties and sources of atmospheric aerosols, as well as their regional differences ~~in the vast TP regions by performing~~, through multiple short-term intensive ~~field~~ observations ~~using~~across this vast region utilizing a suite of high-~~time-~~resolution online instruments. This paper presents a systematic hourly scaled dataset of ~~the high-time-resolution (hourly scales)~~ aerosol physicochemical and optical properties at eight ~~different~~ sites ~~over~~across the TP and its surroundings derived from the ~~observation~~ project~~, including the~~. It includes size-resolved chemical compositions of submicron aerosols, ~~standard~~ high-resolution mass spectra and sources of organic aerosols, size distributions of particle number concentrations, particle light scattering and absorption coefficients, particle light absorptions ~~from~~attributed to different carbonaceous substances ~~of~~including black carbon and brown carbon, and number concentrations of cloud condensation nuclei. In brief, atmospheric aerosols in these remote sites were all well-mixed and highly aged ~~due to~~, reflecting their dominated regional transport sources. However, the southern TP region exhibited high contributions of carbonaceous organic aerosols, neutralized bulk submicron aerosols, and a relatively higher light absorption ~~capability were observed in the southern TP region~~capacity, whereas in the northern TP region, secondary inorganic species ~~contributed dominantly~~were the main contributors to the overall acidic submicron aerosols ~~in the northern TP region. In addition to the~~. Beyond providing insights into the regional differences ~~on~~in aerosol sources and properties ~~in~~across the ~~vast~~ TP ~~regions~~and its surroundings, the datasets ~~are~~will also ~~useful for the simulation~~benefit simulations of aerosol radiative forcing and ~~the evaluation~~evaluations of interactions among different ~~components of the~~ Earth system components in numerical models~~.~~, in

64 this region. The datasets are ~~available from~~accessible through the National Cryosphere

65 Desert   Data   Center,   Chinese   Academy   of   Sciences

66 (https://doi.org/10.12072/ncdc.NIEER.db2200.2022; Xu, 2022).

1 Introduction

Tibetan Plateau (TP), with ~~a mean altitude of over 4000~~an average elevation exceeding 4,000 m above sea level (a.s.l~~.~~) and spanning a ~~huge~~ surface area of approximately 2.5~~×10⁶ km², is the ~~ million square kilometers, stands as the highest plateau on the Earth. ~~The~~Its high-altitude mountain ranges ~~on the TP and its surroundings are~~, integral to one of the world's most ~~important~~crucial cryospheric regions ~~in ~~, have earned the TP the ~~world. Therefore, the TP has been widely known as the ~~monikers "roof of the world", ~~the ~~"Third Pole", ~~or the~~and "Asian Water Tower" (Qiu, 2008; Yao et al., 2019). The TP and its surroundings ~~have significant impacts in~~play a pivotal role in influencing the global and regional climate systems, hydrological cycles, and cryospheric changes through its ~~huge~~vast and complex topography and its function as a significant heat source (Duan and Wu, 2005; Yao et al., 2012; Chen et al., 2021). ~~Over the past few~~In recent decades, ~~one of the most concerns on the TP and its surroundings~~a major concern has ~~been ~~focusing on the significant climatic warming and the rapid ~~cryospheric~~ changes in the cryosphere of this region (Kang et al., 2010), which ~~show~~exhibits a ~~higher ~~warming ~~rate than~~trend that exceeding that of the Northern Hemisphere (0.34 vs. 0.29 °C/decade) (You et al., 2021; Zhou and Zhang, 2021).

~~As ~~Atmospheric aerosols, as one of the most complex and ~~important component~~critical components in the atmosphere, ~~atmospheric aerosols play significant roles in the~~significantly influence climatic warming and cryospheric changes in the TP regions ~~through their~~. They exert crucial direct and indirect effects on ~~solar radiation~~atmospheric energy budget and the albedos of snow and ice surfaces, impacting Earth's climate system (Xu et al., 2009; Kang et al., 2019b). ~~Atmospheric aerosols, particularly the two important~~Notably, light-absorbing carbonaceous aerosols (CAs) ~~of~~such as black carbon (BC) and brown carbon (BrC~~), can~~) directly absorb ~~the ~~solar radiation ~~directly, warm~~, warming the atmosphere~~,~~ and ~~finally lead~~contributing to ~~a ~~positive forcing on Earth's energy budget (Ramanathan et al., 2007; Kopacz et al., 2011). For ~~example~~instance, Li et al. (2018) ~~has simulated~~demonstrated that BC causes significantly ~~higher average~~greater albedo reduction (~46%) and instantaneous radiative forcing (7–64 W m^{-2}) ~~caused by BC than mineral dust that deposited ~~on aged snow ~~in the surface~~surfaces of a TP glacier~~. In addition~~ than mineral dust. Moreover, aerosol particles over the TP ~~also exert significant impacts on~~significantly affect ice cloud properties and cloud development through their semi-direct effects (Liu et al.,

100 2019). ~~Since the direct observation of atmospheric aerosols over~~Given the vast and

101 remote nature of the TP ~~regions is remarkably difficult due to the~~, coupled with its

102 complex topography ~~and~~, meteorology, and harsh environment, ~~the~~*in-situ* observation

103 of atmospheric aerosols poses substantial challenges. Consequently, numerical model

104 ~~simulation~~simulations based on reanalysis data ~~has become one of the most popular and~~

105 ~~critical ways over the past~~have emerged as a predominant and crucial method in recent

106 decades. ~~For example,~~Notable studies include Lau et al. (2006) ~~evaluated~~, who assessed

107 the ~~significant~~ impact of atmospheric aerosols ~~over the TP~~ on the ~~intensification of the~~

108 Asian summer monsoon ~~by~~ intensification using the NASA finite-volume general

109 circulation model~~, of which inputs were driven by the realistic global wind analyses and~~

110 ~~humidity~~; Kopacz et al. (2011) ~~investigated~~, who explored the origin and radiative

111 forcing of BC ~~transported to~~in the TP and Himalayas ~~by using~~with the GEOS-Chem

112 global chemical transport model ~~based on the global BC emissions inventory data;~~; and

113 Liu et al. (2015) ~~investigated~~, who examined the transport of summer dust and

114 anthropogenic aerosols ~~over the TP by~~ using a three-dimensional aerosol transport–

115 radiation model with ~~the~~satellite data inputs. Despite the significant insights gained

116 from ~~diverse satellite remoting products. Although important findings have been~~

117 ~~reported from those numerical model~~ these simulations, ~~the~~ *in-situ*

118 ~~observation~~observations of atmospheric aerosols ~~over the TP regions has become more~~

119 ~~crucial and urgent due to their key roles~~ in the TP are increasingly recognized as critical

120 for evaluating and ~~improving the~~enhancing model ~~performances over the~~accuracy in

121 this remote ~~region. Lacking~~area. The absence of *in-situ* ~~observational~~ aerosol

122 ~~parameters for constraining the model would lead to high~~ data to refine models

123 introduces considerable uncertainty ~~in~~into the results. ~~In addition,~~Furthermore, while

124 model simulations ~~in the TP mostly focused~~primarily focus on ~~the~~ spatial distribution

125 ~~over a large range, but rarely on the~~across broad regions, they often overlook temporal

126 variations or the inherent evolution ~~mechanism with~~mechanisms at high ~~time~~temporal

127 resolution ~~as those from~~, which in-situ observations could illuminate.

128 ~~With great improvements~~Recent advancements in observational ~~conditions~~techniques

129 and ~~instruments,~~instrumentation have enabled numerous *in-situ* ~~measurements have~~

130 ~~been conducted in~~measurement within the TP and its surroundings ~~during~~, aiming to

131 delineate the ~~past few years to characterize the aerosol~~physical, chemical, and optical

132 properties~~,~~ of aerosols, along with their potential sources, transport pathways, and

regional distributions. ~~A comprehensive summary~~A detailed compilation of direct ~~measurements on~~ ambient ~~aerosols~~aerosol measurements in the TP~~using various~~, employing a variety of observational methods and instruments ~~has been listed~~, is presented in Table S1 in the supplementary~~. Among them, the~~ material. Notably, off-line atmospheric filter sampling ~~was one of the most important and popular~~has emerged as a key in-situ aerosol collection ~~approach~~method in the TP~~because it was relatively~~, favored for its low-cost and ~~easy to carry out~~feasibility under the ~~extremely~~region's harsh ~~natural~~ conditions and ~~limit~~ logistical ~~supports~~constraints. This ~~approach~~method has ~~been successfully conducted to characterize the compositions, sizes~~effectively captured the composition, size, light ~~absorptions~~absorption properties, sources, and variations of ambient aerosols, ~~especially those different CAs constituents~~ including diverse CAs components such as BC, BrC, organic carbon (OC), water-soluble OC (WSOC), humic-like substances (HULS), and polycyclic aromatic hydrocarbons (PAHs~~),~~) in the remote TP region (Cao et al., 2009; Zhao et al., 2013; Xu et al., 2014a; Zhang et al., 2014; Cong et al., 2015; Wan et al., 2015; Xu et al., 2015; Kang et al., 2016; Li et al., 2016b; Xu et al., 2020). ~~In addition, characterizing~~Furthermore, off-line filter sampling has been instrumental in mapping the regional aerosol distribution ~~of atmospheric aerosols over a large area of~~across the TP ~~was another important advantage of~~, facilitated by its simplicity and the ~~off-line filter sampling through their~~ability to conduct simultaneous observations at multiple ~~sites due to the relatively easy instrumental operations~~locations (Li et al., 2016a; Chen et al., 2019; Kang et al., 2022). ~~However, studies on the atmospheric aerosols over the remote TP regions through~~Despite these advancements, off-line filter ~~samplings are still scarce and far meeting the demand at present. These observational~~ sampling studies in the TP's remote regions remain insufficient for current needs. The gathered data ~~was~~is generally ~~scattered~~fragmented and unsystematic~~with relatively~~, characterized by low ~~time~~temporal resolution, ~~few~~limited aerosol property parameters, and ~~less~~sparse data points ~~because most of them were carried out at certain site using~~. Typically, these studies have been localized to specific sites, utilizing single instruments with ~~time~~temporal resolutions ranging from days to weeks ~~during a short-term period. The~~ over brief periods. Such low ~~time~~temporal resolution ~~measurement would limit~~limits the accurate understanding of aerosols' temporal evolution ~~processes~~ and underlying mechanisms ~~of aerosol properties~~, especially during ~~a fast and~~rapid, short-term ~~event. Meantime, these observational~~events. Additionally, integrating and comparing data

~~from~~across different research groups ~~was also difficult to compare and integrate~~ ~~because most of them had different~~is challenging due to variations in research ~~concerns,~~ ~~measurement~~focuses, measured parameters, sampling ~~flows~~methodologies, laboratory filter ~~treatment procedures,~~ processing, and data analysis ~~methods, etc. Besides,~~ ~~although the~~ techniques. Moreover, despite the relative ease of off-line sampling ~~is~~ ~~relatively easy to carry out, there are still large TP regions where similar observations~~ ~~have not yet been conducted or only conducted in a short term period. Up to now,~~ extensive areas of the TP still lack such observational efforts. To date, comprehensive research focusing on multiple aerosol ~~physicochemical and optical~~ ~~properties~~parameters through ~~the~~ real-time online consecutive measurements (with high temporal resolutions from minute to hour scales) at multiple sites ~~are still~~ ~~rare~~remains a rarity in the TP.

~~Studies~~Research on atmospheric aerosols ~~have~~in China has achieved ~~great progress~~ ~~during~~significant advancements over the ~~last~~past decade ~~in China~~. The Aerodyne high-resolution time-of-flight aerosol mass spectrometer (HR-ToF-AMS) ~~was one of the~~ ~~most popular~~has become a widely used online instrument ~~that successfully~~ ~~implemented in~~, enabling numerous ~~aerosol chemistry observations~~studies to characterize the real-time, size-resolved chemical compositions and sources of submicron aerosols (Li et al., 2017; Zhou et al., 2020). However, ~~the utilization of HR-~~ ~~ToF AMS on~~its application in the TP ~~was still very scarce due~~has been limited, a situation attributed to the ~~high instrumental~~instrument's demanding operational requirements ~~but extremely harsh~~and the area's challenging observation conditions. Since 2015, our research group has initiated a continuous and systematic observation project, aiming to investigate the regional differences on aerosol sources and properties ~~in~~across the ~~different~~ TP ~~regions, has been launched by our research team by performing~~. This effort involves annual deployments of the HR-ToF-AMS ~~measurement~~ ~~and~~alongside other high-resolution, real-time online instruments at ~~different~~various sites ~~during almost every year. Indeed~~. Remarkably, our dataset ~~was~~represents the first and only ~~set of dataset focusing on abundant~~ collection that extensively covers a wide range of aerosol parameters (including ~~the~~ physical, chemical, and optical properties and their diverse sources) ~~at~~across multiple ~~different types of site~~geographic environments (e.g., ~~the~~ urban, remote, high-altitude mountain, grassland, and subtropical forest ~~sites that basically represented the different TP regions) based on the~~)

within the TP and its surroundings. This is achieved through real-time and high-time-resolution online observations, providing a comprehensive resource for understanding regional aerosol variations and serving as essential input for future aerosol radiative forcing simulations and Earth system interaction assessments. The structure of this paper is as follows: Sections 2 and 3 describe the observation sites, instrumental deployments, and data processing. Section 4 presents the high-time-resolution aerosol data, encompassing physical, chemical, and optical properties as well as source information. The limitations and the uniqueness of our dataset are discussed in Section 5.

2 Observation site descriptions

Between 2015 and 2022, intensive observations of atmospheric aerosol chemistry were carried out at eight sites across the TP and its surroundings. These sites comprise seven remote sites (QOMS, Motuo, NamCo, Ngari, Waliguan, LHG, and Bayanbulak) and one urban site (Lhasa), the latter serving as a contrast for comparative analysis. Figure 1 illustrates the geographical locations of these sites along with photographs during each observation. Table 1 details the specifics of each site including the sampling periods and the instruments deployed during each field campaign. The subsequent sections provide brief descriptions these sites, arranged geographically from the southern to the northern parts of the TP.

2.1 QOMS

The Qomolangma Station for Atmospheric and Environmental Observation and Research, Chinese Academy of Sciences (86.56ºE, 28.21ºN; 4276 m a.s.l.; abbreviated as QOMS in this study, with similar abbreviations for other sites hereafter), is situated in the Rongbuk valley basin on the northern slope of Mt. Everest. The climate in the

northern slope of Mt. Everest has obvious seasonal variation ~~under~~, heavily influenced by the ~~influence of~~ Indian monsoon system (Bonasoni et al., 2010; Cong et al., 2015). During the pre-monsoon season (~~generally~~typically March~~=~~ to May), ~~the dominated~~dominant westerlies ~~play important roles in~~facilitates the long-range transport of atmospheric pollutants from ~~those polluted regions in~~ South Asia, ~~which makes~~making QOMS an ideal high-altitude observatory ~~at~~on the south edge of the TP for ~~studying the~~examining transboundary pollutant transport ~~of atmospheric pollutants from South Asia to~~into the ~~inner TP. During~~plateau's interior. In the summer monsoon season ~~in summer~~ (June−August), ~~the~~prevailing southerly winds ~~prevail and~~ bring warm and wet airflow from the Indian Ocean, leading to ~~this region with increasing~~increased humidity and precipitation in the plateau.

2.2 Motuo

Motuo ~~county is~~County, located in the lower reaches of the Yarlung Tsangpo River ~~and~~on the southern ~~slope~~slopes of the eastern Himalayas and Gangrigab Mountains in the southeast edge of the TP. The county ~~sits at a~~, sited halfway up a mountain ~~and has~~, enjoys a subtropical humid climate ~~with~~characterized by relatively high ~~temperature~~temperatures and abundant rainfall. ~~Due to the minor~~With a small population (~~~~of ~15,000)~~,~~, Motuo ~~county is also a relatively~~County remains one of the TP's most pristine ~~region in the TP.~~regions. The sampling site in Motuo (29.30°N, 95.32°E; 1305 m a.s.l.) was ~~at the summit of~~located atop a hill ~~that towards too~~overlooking the Yarlung Tsangpo Grand Canyon~~, which~~. This vantage point makes it ~~a very~~an ideal ~~site in the southeast edge of the TP to~~location for directly ~~monitor~~monitoring the transboundary transport of atmospheric pollutants and moisture from Southeast Asia and the Indian Ocean ~~to~~into the TP.

2.3 NamCo

The Nam Co Station for Multisphere Observation and Research, Chinese Academy of Sciences (NamCo; 90.95ºE, 30.77ºN; 4730 m a.s.l.) is a high-altitude observatory ~~at~~in the south-central part of the TP. ~~This station is situated~~Situated at the southeast shore of Nam Co Lake~~. The surrounding of this~~, the station is surrounded by a pristine ~~region in the TP~~ and isolated ~~from major populated areas.~~area. The region ~~is generally affected by the~~experiences a typical semi-arid plateau monsoon climate~~ with more~~, characterized by increased precipitation during the summer monsoon season. ~~The~~

264 NamCo is ~~the most important site in~~a pivotal inland ~~of~~site within the TP~~and dominated,~~

265 predominantly influenced by air ~~mass~~masses from the south and west.

2.4 Ngari

267 The Ngari Station for Desert Environment Observation and Research, Chinese

268 Academy of Science (Ngari; 79.70°E, 33.39°N; 4270 m a.s.l.) ~~locates~~is located in the

269 Rutog County~~,~~ within the Ngari Prefecture~~,~~ of the Tibet Autonomous Region, China.

270 This ~~region~~area is at the southwestern edge of the TP and ~~belongs to~~is characterized by

271 its semi-arid ~~areas with barren land surface~~climate, sparse vegetation, and ~~strong~~intense

272 solar radiation. As ~~the major~~a key member of ~~the~~ "high-cold region observation and

273 research network for land surface processes & environment of China", the Ngari station

274 ~~is one of the most important filed stations for~~plays a crucial role in monitoring ~~the~~

275 ~~changes in~~ climate, ~~hydrology, atmosphere~~hydrological, atmospheric, and ecological

276 ~~environment~~environmental changes in the TP's western ~~region of the TP and further~~

277 ~~revealing the interaction~~territories. Additionally, it contributes to understanding the

278 interactions between the Indian monsoon system and the ~~westerly belt~~westerlies.

2.5 Waliguan

280 The Waliguan Baseline Observatory (Waliguan; 100.9ºE, 36.28ºN; 3816 m a.s.l.) is one

281 of the twenty-nine baseline stations of Global Atmosphere Watch (GAW) ~~of~~under the

282 World Meteorological Organization (WMO). ~~The observatory is situated~~Situated at the

283 top of ~~the~~ Mt. Waliguan ~~(mountain height of ~600 m),~~, which ~~is also a relatively~~rises

284 approximately 600 m, the observatory is located in a pristine region with ~~little influence~~

285 ~~from~~ minimal human ~~activities. The~~activity impact. Waliguan is ~~an~~

286 ~~important~~represented as a key observatory ~~in~~on the ~~northeast~~northeastern edge of the

287 TP~~and dominated~~, predominantly influenced by air ~~mass~~masses from the northeast

288 during the summer ~~season, which makes it an ideal site to study the influence~~. This

289 location is strategic for studying the transport and impact of air pollutants from ~~the~~

290 industrial ~~areas~~regions in ~~the~~ northwestern China to the TP in this study.

2.6 LHG

292 The Qilian Observation and Research Station of Cryosphere and Ecologic Environment,

293 Chinese Academy of Sciences (LHG; 39.50°N, 96.51°E; 4180 m a.s.l~~.) locates near~~

294 ~~the~~.), is located approximately 1km from the terminus ~~(~1 km)~~of ~~the~~ Laohugou Glacier

295 No.12~~, which~~. This glacier is ~~one~~among the largest mountain glacier in the northern

296 slope of the western Qilian Mountains. LHG ~~is~~serves as another ~~representative~~notable

297 station in the northeastern TP ~~and significantly isolated~~, distinctly remote from ~~the~~

298 human ~~living areas~~settlements. The climate in this region is ~~a typically~~predominantly

299 arid and continental ~~climate and dominated~~, influenced by the East-Asian monsoon in

300 ~~the~~ summer and the Westerlies in ~~the~~ winter. ~~Strongly~~A pronounced mountain-valley

301 breeze ~~is formed~~ during summer ~~which can bring air mass~~facilitates the upward

302 transport of air masses from lower ~~altitude zones to mountain regions. Therefore, it is~~

303 ~~also well suited~~altitudes, making LHG an ideal site for ~~sampling the~~ background air

304 mass sampling and ~~studying~~for investigating the transport ~~mechanisms~~ and potential

305 impacts of air pollutants from ~~its~~ surrounding ~~regions~~areas.

2.7 Bayanbulak

307 The Bayanbulak National Basic Meteorological Station (Bayanbulak; 84.35° N, 42.83°

308 E; 2454 m a.s.l.) ~~locates~~is located in the Bayanbulak grassland ~~at the~~, northwest of

309 Hejing ~~county,~~County in the Xinjiang Uygur Autonomous Region, China. ~~The~~

310 Bayanbulak ~~is situated in~~lies within an intermontane basin in the central Tianshan

311 Mountains ~~and~~, surrounded by numerous snow mountains with altitudes more than

312 3000 m. The climate in Bayanbulak grassland ~~belongs to the~~is characterized by a typical

313 temperate continental mountain climate, with an annual average precipitation ~~of~~

314 ~~about~~ranging between 200 ~~–~~ to 300 mm. ~~The~~ Bayanbulak town ~~has limited~~experiences

315 minimal human activities and traffic ~~transportation~~, maintaining its pristine

316 environment.

2.8 Lhasa

318 Lhasa (29.65°N, 91.03°E; 3650 m a.s.l.) is the capital ~~city~~ of the Tibet Autonomous

319 Region, China ~~that~~, and located in the south-central part of the TP. The city lies in a

320 ~~flat~~broad river valley ~~with the surrounding~~, surrounded by mountains ~~reaching~~ that

321 reach up to 5500 m ~~and~~, with the Lhasa River passing through the city from west to

322 east. ~~The~~Our observation site is located in ~~Lhasa is in the~~ Binhe Park ~~near~~, adjacent to

323 the Lhasa River. ~~The~~Notably, the Norbulingka scenic area, one of the main activity

324 centers for local Tibetans ~~to celebrate~~celebrating their religious festivals ~~(e.g.,~~such as

325 the Sho Dun festival~~),~~, is located ~1 km to the northwest of the sampling site~~, while~~.

326 Moreover, the Potala Palace, the center of Tibetan Buddhism, is ~1.8 km to the northeast.

327 ~~Since the~~Given Lhasa's unique energy structure and ~~different residential habit in Lhasa~~

comparing with those remote sites, a~~the distinct living habits of the residents,~~
comparative ~~observation is conducted in~~observations are carried out at this urban site
~~for studying~~. These studies aim to investigate the primary aerosol properties and sources,
particularly from various residential combustion activities.

3 Online sampling, instrumental setup, and data processing

3.1 Online real-time aerosol sampling over the TP

~~The online based~~ Atmospheric aerosol observations ~~of atmospheric aerosols~~ were
~~carried out~~conducted at each site using a ~~suit~~suite of real-time, high-resolution
instruments~~, usually including~~. This instruments typically included a HR-ToF-AMS
(Aerodyne Research Inc., Billerica, MA, USA) ~~for acquiring~~to determine the chemical
~~compositions~~composition (organic aerosol (OA), nitrate, sulfate, ammonium, and
chloride) of non-refractory submicron aerosol (PM_1~~), a~~); A scanning mobility particle
sizer (SMPS, model 3936, TSI Inc., Shoreview, MN, USA) ~~for acquiring~~was used to
measure the size distribution ~~of~~and number concentration of submicron particles~~, a~~; A
photoacoustic extinctiometer (PAX, DMT Inc., Boulder, CO, USA) was used for
~~acquiring the~~obtaining particle light absorption, scattering, and extinction coefficients
(Babs, Bscat, and Bext) ~~and~~along with single scattering albedo (SSA) at 405 nm, as
well as ~~the~~BC mass concentration ~~of BC, an~~; An Aethalometer (model AE33/AE31,
Magee Scientific Corp., Berkeley, CA, USA) was used for acquiring the B_{abs} ~~at~~across
seven ~~fixed~~ wavelengths (370−950 nm~~), and a~~); A cloud condensation nuclei (CCN)
counter (model CCN-100, DMT Inc., Boulder, CO, USA) ~~for acquiring the~~measured
CCN number ~~concentration at different supersaturation (SS) of~~concentrations at various
water vapor~~.~~ supersaturations (SS). The measurement uncertainties for each instrument
are difficult to quantify based on data from a single instrument. The uncertainty
showing below are referred from other studies: <30% for HR-ToF-AMS (Jimenez et al.,
2016) and SMPS, <40% for Aethalometer (Backman et al., 2017), <10% for PAX
(Selimovic et al., 2018), and <25% for CCNC (Rose et al., 2008). Details on the specific
~~instrumental deployment~~instruments deployed and the sampling ~~period during~~periods
for each observation campaign ~~is~~are summarized in Table 1.

The HR-ToF-AMS~~, serving as~~ was the ~~primary~~cornerstone instrument for ~~observing~~
atmospheric aerosol chemistry~~, was deployed throughout~~ observations across all field
campaigns. The SMPS was ~~utilized~~deployed at QOMS, Motuo, LHG, and Lhasa,
~~while~~whereas the PAX was employed at QOMS, Motuo, Ngari, Waliguan, and Lhasa.

361 ~~Additionally, the~~The Aethalometer was utilized at QOMS, NamCo, and Waliguan,
362 ~~and~~with the CCN-100 operational at Motuo, Waliguan, and LHG. Field observations in
363 the southern, western, ~~or~~and central ~~TP~~ regions of the TP were predominantly
364 conducted during the pre-monsoon ~~periods.~~ season, aimed to study the transboundary
365 transport of pollutants from South Asia into the TP, under the influence of Westerlies
366 and the Indian monsoon. For instance, observations took place from 12 April to 12 May
367 at QOMS, Motuo from 26 March to 22 May ~~at Motuo,~~, NamCo from 31 May to 1 July
368 ~~at NamCo~~, and Ngari from 1 Jun to 5 July ~~at Ngari, which were to investigate the~~
369 ~~transboundary transport of atmospheric pollutants from polluted regions in South Asia~~
370 ~~to the inland areas of the TP, considering the influences of Westerlies and the Indian~~
371 ~~monsoon. .~~ On the other hand, measurements in the remote regions of the northern TP
372 and its surroundings were carried out during the summer~~.~~ to track aerosol transport
373 from surrounding polluted areas, considering the effects of the Westerlies or the
374 intensified East Asian monsoon. Specifically, observations occurred from 1 to 31 July
375 at Waliguan, from 4 to 29 August at LHG, and from 29 August to 26 September at
376 Bayanbulak. ~~These measurements were undertaken to monitor the aerosols transported~~
377 ~~from surrounding polluted regions, considering the influences of Westerlies or the~~
378 ~~intensified East Asian monsoon.~~ The observation ~~in~~at Lhasa was conducted
379 ~~between~~from 31 August ~~and~~to 26 September, focusing on capturing the ~~strongest~~peak
380 atmospheric oxidation ~~capability~~capacity during the summer~~ season~~.

3.2 Instrumental setup

382 Despite the variations in ~~the instruments used during~~instrumentation across different
383 observation campaigns, the core setup for sampling ~~settings remain generally~~was
384 largely consistent. Figure 1b illustrates the ~~fundamental~~standard sampling ~~setup~~
385 ~~employed~~configuration for each campaign~~. All instruments are~~ typically ~~housed~~
386 involved housing all instruments within an air-conditioned trailer or room. The inlets
387 ~~are~~were induced to the instruments from the roof with a ~~fine particle~~ cyclone (model
388 URG-2000-30EH, URG Corp., Chapel Hill, NC, USA) in the front of the inlet to
389 eliminate particles with an aerodynamic diameter (D_{va}) exceeding 2.5 μm. ~~Subsequently,~~
390 ~~the~~These fine particles ~~are directed into~~ were then passed through a Nafion dryer via
391 1/2-inch stainless steel ~~tubes~~tubing to ~~remove moisture from~~dehumidify the airflows~~.~~
392 ~~Lastly, the particles are sampled into a series of online~~ before being directed into the
393 instruments for real-time ~~measurements~~analysis. For ~~a more comprehensive~~

394 ~~understanding~~detailed information on the setup and methodology of the ~~instrumental~~

395 ~~setups, please refer to~~instruments, it can be found in our previous publications (Xu et

396 al., 2018; Zhang et al., 2018; Zhang et al., 2019; Zhao et al., 2022).

3.3 Instrumental operation and data processing

The measurement principles, operation procedures, calibration methods, and data
analysis for these instruments ~~are extensively described~~used in ~~detail~~this study are
thoroughly detailed in ~~Text~~Texts S1−~~4 in the~~S4 of supplementary ~~materials of this study.~~
~~Only a few essential~~material. Here, we highlight only key descriptions and ~~important~~
~~settings are emphasized here~~critical setting as follows: (1) The HR-ToF-AMS
~~instruments were~~was operated at ~~the~~ V-mode during ~~almost all~~most of the eight field
campaigns~~, considering~~ to accommodate the relatively low ~~aerosol mass levels and~~
signal-to-noise ratios ~~over~~due to low aerosol mass loading in the TP regions. (2) ~~Due to~~
~~chopper malfunction in the HR-ToF-AMS, particle~~Particle size observations were not
conducted during the NamCo and LHG campaigns~~.~~ due to a chopper malfunction in the
HR-ToF-AMS. (3) Different relative ionization efficiency (RIE) values were used for
ammonium and sulfate according to the ionization efficiency calibrations of HR-ToF-
AMS in different campaigns~~, while default values were used to rest species.~~. (4)
Different size parameters were achieved according to the particle sizing calibrations in
different campaigns~~, which ultimately resulted in the distinct size ranges of non-~~
~~refractory PM₁.~~. (5) Elemental ratios of OA~~, i.e.,~~ such as oxygen-to-carbon (O/C),
hydrogen-to-carbon (H/C), organic matter-to-organic carbon (OM/OC), and nitrogen-
to-carbon (N/C), were determined using the improved method (Canagaratna et al.,
2015). (6) ~~Default~~A default collection efficiency (CE) ~~values~~value of 0.5 were
employed to the HR-ToF-AMS measurements during the QOMS, NamCo, Ngari,
Waliguan, and Lhasa campaigns in consideration of their overall neutralized bulk
submicron aerosols, whereas ~~the~~a composition-dependent CE (Middlebrook et al., 2012)
~~values are~~value was adopted at Motuo, LHG, and Bayanbulak, where ~~bulk submicron~~
aerosols were slightly acidic. (7) Source ~~apportionments~~apportionment of OA during
all observations were performed by the positive matrix factorization (PMF) analysis
~~method.~~. The details of the PMF solution determination for each site are not presented
here but can be referenced in our previous publication for select campaigns (Xu et al.,
2018; Zhang et al., 2018; 2019). (8) Only the chemical compositions of non-refractory
PM₁ are reported ~~during~~for the Bayanbulak campaign due to the absence of BC

427 observations. (9) The sample and sheath flow rates of SMPS were set at 0.3 and 3.0 L

428 min^{-1}, respectively, at both QOMS and Lhasa, ~~measuring particles~~covering a particle

429 size range between 14.6 and 661.2 nm in mobility diameter (D_m), whereas 0.5 and 5.0

430 L min^{-1} at LHG and Motuo sites with a ~~particle size~~ range of 10.9−495.8 nm in D_m. (10)

431 Aethalometer ~~measurement~~measurements were corrected for ~~both the~~ filter-based

432 loading ~~effect~~ and multiple scattering ~~effect~~effects. A traditional absorption Ångström

433 exponents (AAE) method (Zhang et al., 2021) was adopted to ~~quantitatively~~ apportion

434 ~~the~~ total B_{abs} into two parts ~~from~~of BC and BrC ($B_{abs,BC}$ and $B_{abs,BrC}$). (11) ~~During the~~

435 ~~Motuo, Waliguan, and LHG campaigns, the~~ CCN number concentrations ~~of CCN~~ were

436 ~~conducted consecutively~~measured at five different SS values of 0.2%, 0.4%, 0.6%,

437 0.8%, and 1.0% ~~every 5 minutes~~at a 30-min cycle during the Motuo, Waliguan, and

438 LHG campaigns.

4 Aerosol properties, sources, and radiative forcing over the TP

4.1 Mass loading and chemical composition of submicron aerosols

441 Figure S1 ~~provides an overview of the high-time-resolution~~presents the temporal

442 variations of PM$_1$ chemical species (OA, nitrate, sulfate, ammonium, chloride, and BC)

443 ~~during~~observed across the eight observations in the TP and its surroundings. ~~Generally,~~

444 ~~the~~ The mass concentrations of PM$_1$ and its ~~chemical species varied~~

445 ~~dynamically~~components exhibited distinct variations, with ~~alternating~~a few periods of

446 high ~~and low~~ mass loading observed throughout ~~the~~each campaign's sampling period

447 ~~of each campaign.~~. Despite ~~differences~~variations in sampling years (2015−2022),

448 seasons (March−September), and altitudes (1350−4730 m a.s.l.) ~~at~~across these sites, the

449 ~~significantly~~ distinct PM$_1$ mass concentrations and chemical compositions ~~can~~

450 ~~effectively reflect~~clearly illustrate the regional difference ~~in aerosol mass levels,~~

451 ~~properties, and sources at different regions.~~among these sites. On average, ~~the mass~~

452 ~~concentration of~~total PM$_1$ mass concentrations across the eight campaigns ranged from

453 1.9 to 9.1 µg m^{-3} (Fig. 2 and Table 2). The highest ~~PM$_1$~~ mass concentration was

454 observed at Waliguan ~~due to~~, driven by the ~~rapid~~ transport of anthropogenic aerosols

455 and gaseous pollutants from urban ~~areas~~centers in northwestern China. ~~Conversely~~In

456 contrast, the lowest values were ~~measured~~observed at NamCo and Bayanbulak,

457 ~~attributed to~~reflecting their background and pristine environmental conditions. The

458 average PM$_1$ mass level ~~in~~across the TP and its surroundings was comparable to

459 ~~values~~those observed at other high-altitude, coastal, forest, and remote background sites

460 ~~worldwide~~globally (0.46−15.1 µg m^{-3}; Table 3), ~~but~~yet remains significantly lower than

461 those observed at densely urban (34.4−71.5 µg m^{-3}) and suburban (21.4−44.9 µg m^{-3})

462 ~~sites~~areas in other ~~regions~~parts of China (Li et al., 2017)~~, suggesting~~. This suggests the

463 predominantly clean ~~nature of atmosphere condition~~atmospheric conditions in the

464 remote and high-altitude regions of the TP.

465 The chemical compositions of PM$_1$ also exhibited significant regional ~~difference~~

466 differences across the TP (Fig. 2), ~~indicating distinct~~highlighting varied aerosol sources

467 ~~across~~in different ~~TP regions. OA and BC together contributed as high as~~

468 ~~64.9−85.7%~~areas of the ~~total PM$_1$ mass at the~~TP. At five sites ~~of~~(QOMS, Motuo,

469 NamCo, Ngari, and Lhasa ~~that are~~) located in the southern, western, or central TP~~-~~, OA

470 and BC together accounted for as high as 64.9−85.7% of the total PM$_1$ mass (Table 2).

471 ~~These~~This high ~~contributions were mainly~~contribution was largely attributed to the

472 frequent transport of biomass-burning ~~related~~ emissions from ~~polluted regions in~~South

473 and Southeast Asia to the ~~remote sites of~~ TP during the pre-monsoon season (Bonasoni

474 et al., 2010; Cong et al., 2015; Zhang et al., 2018)~~ as well as the intense~~, along with

475 significant local biomass burning ~~emissions~~ from religious activities in ~~the urban area~~

476 ~~of~~Lhasa (Cui et al., 2018; Zhao et al., 2022). In ~~contrary,~~contrast, at the three northern

477 sites (Waliguan, LHG, and Bayanbulak), inorganic species (sulfate, nitrate, and

478 ammonium; referred to as SNA) accounted for more than 60% of the total PM$_1$ ~~at three~~

479 ~~northern sites (Waliguan, LHG, and Bayanbulak). Among these, sulfate had~~. Sulfate

480 was the most ~~dominant contributions~~significant component of SNA (38.1−46.0%),

481 ~~consistent~~aligning with ~~the results observed at~~observations from another high-altitude

482 site in the northeastern TP (Menyuan; 28%) and ~~other~~various rural and remote sites

483 (19–64%) in East Asia~~, indicating the regional transported sources~~ (Du et al., 2015).

484 The ~~high~~pronounced SNA contributions ~~of SNA~~, particularly ~~the~~sulfate, in the northern

485 TP and its surroundings~~,~~ were mainly related to the regional transport of anthropogenic

486 aerosols and gaseous precursor ~~emissions~~ from ~~surrounding~~nearby urban areas as well

487 as important in-cloud aqueous reactions during the transportation to the mountains

488 (Zhang et al., 2019).

489 **4.2 Bulk acidity, size distribution, and diurnal variation of submicron aerosols**

490 Particle phase acidity ~~is an important parameter affecting the~~significantly influences

491 aerosol physicochemical properties ~~of aerosol, with significant impacts on hygroscopic~~

492 ~~growth~~, affecting hygroscopicity, toxicity, and heterogeneous reactions ~~of aerosol~~

~~particles~~. The bulk acidity of submicron aerosols was evaluated at each site following the method in Zhang et al. (2007b) and Schueneman et al. (2021) ~~based on~~using AMS measurements. A detailed description of this method can be found in Text S5 of the supplementary material or our previous publications (Zhang et al., 2018; Zhang et al., 2019)~~or in Text S5 in the supplementary materials of this study. It is interesting to find that the bulk acidity of submicron aerosols exhibited distinct~~. Notably, we observed clear regional ~~difference~~variations between the southern and northern TP ~~(Fig. 3), primarily attributed to variations~~, largely due to differences in aerosol sources and ~~compositions.~~composition (Fig. 3). Linear regression slopes ~~were fitted to be 1.2, 1.11, 0.98, and 1.18 at the four sites of~~at QOMS, NamCo, Ngari, and Lhasa ~~that locates~~(located in the southern, western, or central TP) were fitted to be 1.2, 1.11, 0.98, and 1.18, respectively, indicating the submicron ~~aerosol particles~~aerosols at these sites were generally neutralized, ~~and in some cases, showed~~occasionally showing an excess of ammonium. The ~~finding~~result is consistent with previous ~~observations of~~findings on high ammonia availability ~~resulted~~ from agriculture emissions in the South Asia (Van Damme et al., 2015). ~~In addition~~Moreover, as reported in our previous publications, atmospheric aerosols at QOMS and NamCo were significantly influenced by ~~the transport of~~ biomass-burning ~~related~~ emissions from South and Southeast Asia during the pre-monsoon season (Xu et al., 2018; Zhang et al., 2018), ~~while various residential~~and Lhasa experienced intense biomass ~~fuels were burned intensely~~fuel burning during ~~those~~ frequent religious festivals ~~in urban areas of Lhasa~~ (Zhao et al., 2022). In contrast, ~~the~~ submicron particles at the remaining four sites, particularly LHG and Bayanbulak in the north, were overall acidic, with regression slopes ranging from 0.73 to 0.86 ~~at the remaining four sites, especially in the two northern sites (LHG and Bayanbulak),~~, where sulfate ~~significantly contributed to the total~~was a major PM$_1$ component (46.0% and 41.6%). Similar ~~observations~~findings of acidic submicron aerosol particles have also been observed at Menyuan and LHG in the northern TP in previous studies (Du et al., 2015; Xu et al., 2015), mainly related to the transport of ~~the~~ enriched SNA species or their gaseous precursors from the industrial areas in northwestern China ~~to the remote regions in the northern TP~~.

The size distributions of non-refractory PM$_1$ chemical species, obtained from HR-ToF-AMS measurement, provide valuable insights into aerosol sources, oxidation degrees, mixing states, formation, transformation, and growth mechanisms as well as their

impacts on CCN activity. Typically, ~~the~~ size distributions for SNA species and oxidized OA peaked ~~at~~in the accumulation mode (~400−600 nm in D_{va}~~) for those SNA species and oxidized OA components~~), as a result of ~~their~~ secondary formation processes. In contrast, fresh organics from primary emission sources ~~had~~exhibit smaller ~~sizes~~size (Zhang et al., 2005b; Aiken et al., 2009). In this study, ~~both~~we focus on organics and the ~~sum of~~combined three SNA species ~~were selected~~ to ~~illustrate the~~highlight regional ~~difference~~variations in size distributions across the ~~different~~ TP ~~regions~~. As shown in Figs. 4a and S2 and Table 2, the peak diameters ~~in the size distribution~~ of OA and SNA size distributions varied significantly, ~~ranging~~ from 584.4 and 634.5 nm at Ngari to a smaller size of 228.1 and 250.0 nm at Lhasa, respectively. This variation suggests the distinctly different sources and aging processes of atmospheric aerosols ~~in different~~across the TP ~~regions~~, particularly between those high-altitude remote sites and urban sites. For ~~example~~instance, bulk PM$_1$ at QOMS was reported to be internally well-mixed and aged ~~at QOMS due~~, attributed to long-range transport ~~aerosol sources of~~ from biomass-burning~~-related~~ emissions ~~from~~in South Asia (Zhang et al., 2018), whereas local primary sources~~,~~ including cooking, traffic exhausts, and biomass burning ~~together contributed~~, totally accounted for more than 60% of the total OA ~~at the~~in urban ~~site in~~Lhasa (Zhao et al., 2022). The crucial influence of aerosol sources on size distributions is further supported ~~in Fig. 4a~~ by the ~~quantitative relationship~~correlation between the mode size and O/C ratios of OA ($R^2 = 0.74$) (Fig. 4a).

The diurnal variations of PM$_1$ chemical compositions are typically influenced by multiple factors, including ~~the~~ meteorological conditions (~~such as~~e.g., planetary boundary layer (PBL) height, wind direction and speed, temperature, relative humidity), ~~different~~various primary emission sources (~~such as intense~~e.g., vehicle exhausts during traffic rush hours, cooking emissions, and coal combustion emissions ~~from~~for heating ~~activities~~), and distinct formation mechanisms (~~such as~~e.g., daytime photochemical oxidation~~ processes~~, nighttime heterogeneous reactions, and gas-particle partitioning of secondary species). ~~Therefore, a~~A comprehensive understanding of ~~the~~these diurnal ~~variation characteristics of different aerosol chemical compositions~~ variations is ~~not only beneficial~~crucial for ~~investigating their~~ exploring the dynamic evolution ~~processes but also helpful in understanding~~of aerosol compositions and identifying the ~~key factors~~primary drivers (source, meteorology, or secondary formation) ~~that drive~~behind

~~Clearly, different~~ the variations ~~of~~in different chemical species.

Distinct diurnal ~~variation~~ patterns ~~of~~in the total PM$_1$ mass concentrations were observed ~~during the~~across different field campaigns (Fig. 4b). ~~The diurnal variations at those~~ At remote sites ~~(such as~~of QOMS, LHG, NamCo, and Waliguan~~)~~, located ~~either~~ in ~~the valley~~valleys or ~~at the top of the~~atop mountains, variations were ~~mostly controlled~~largely governed by ~~the circulation of~~ mountain-valley wind circulation and ~~the variation of~~change in PBL height ~~during the day.~~. For instance, QOMS exhibited a distinct diurnal pattern with continuously decreasing concentrations during the daytime, but relatively higher concentrations at night. The minimum ~~mass~~ occurred at around ~15:00 in this valley site, ~~mainly~~likely due to ~~the~~ strong ~~down-slope~~afternoon glacier winds ~~with high wind speed~~ and ~~enhanced~~a higher PBL ~~height in the afternoon~~ (Zhang et al., 2018). Conversely, LHG and NamCo experienced lower PM$_1$ ~~mass concentration~~concentrations from night to early morning ~~and continuously increasing concentrations during the afternoon were observed at LHG and NamCo sites. The high mass concentrations~~, with increase in the afternoon, attributed at LHG ~~were tightly associated with the~~to up-slope wind transport ~~of~~and at NamCo to aerosols ~~advected by the prevailing up-slope winds during that time. However, the high concentration in the afternoon at NamCo might be influenced by the downward transmission of aerosols~~descending from higher ~~layer to the ground surface, as well as~~layers and enhanced ~~aerosol plume~~ afternoon transport from ~~those relatively polluted western regions during the afternoon~~the west (Xu et al., 2018). A ~~relatively~~ complex diurnal ~~variation~~pattern of ~~total~~ PM$_1$ was observed at ~~the top of Mt.~~ Waliguan, ~~which could be attributed to the combined effects of variabilities in~~influenced by diffusion conditions ~~(such as PBL height)~~, wind directions ~~(such as mountain-valley wind circulation)~~, and air mass sources ~~(such as enhanced~~, including afternoon air ~~mass~~masses from the northeast ~~during the afternoon, favoring the transport of polluted aerosols from~~, which likely carried industrial ~~areas)~~pollutants (Zhang et al., 2019). At Motuo, the diurnal ~~variation~~pattern of PM$_1$ ~~mass concentration~~ was relatively stable, ~~except for~~with two weak peaks linked to local combustion activities in the late morning and evening, ~~which were possibly related to combustion emissions from local residents in the county.~~. Ngari exhibited relatively ~~high mass~~higher nighttime loadings ~~at night, whereas low values were observed during the~~and lower daytime loadings, mainly due to the variations of PBL height. Bayanbulak, on the other hand, had relatively low and stable PM$_1$ mass

throughout the entire day~~, primarily~~ due to its background ~~feature~~location. In contrast ~~to the remote sites, the~~, urban ~~site in~~ Lhasa ~~showed a clear diurnal variation pattern with~~ displayed two pronounced peaks ~~around 8:00–9:00 and 20:00–21:00. This pattern could be attributed to strong~~correlating with primary ~~aerosol~~ emissions ~~from vehicle exhausts, cooking, and biomass burning activities~~ during ~~the~~ morning and evening ~~times~~rush hours (Zhao et al., 2022). Although the diurnal ~~variations~~pattern of ~~total~~ PM$_1$ were mainly ~~affected~~shaped by ~~the variabilities in~~ mountain-valley ~~wind circulation~~winds and PBL height in those remote sites~~,~~ and primary emissions in the urban site in this study, ~~the~~secondary formation processes, including photochemical oxidation and aqueous-phase reactions were also ~~two important~~played a key role in the formation ~~pathways~~ of ~~secondary~~ inorganic and organic aerosol species. This could be ~~observed clearly~~evidenced by ~~those identified~~the afternoon peaks of oxygenated OA (OOA) components ~~at~~observed across almost all the sites, which were commonly ~~showed peaks during the afternoon~~formed by photo-chemical processes (Xu et al., 2018; Zhang et al., 2018; Zhang et al., 2019; Zhao et al., 2022).

4.3 High-resolution mass spectrum and elemental ratios of organic aerosol

The high-resolution mass spectrum (HRMS) and elemental ratios of OA were determined to identify the possible sources, formation and evolution mechanisms, ~~as well as the~~and oxidation states ~~of these complex OA components~~ at each site. ~~The~~A direct comparison of the average O/C ratios ~~of the OAs~~ from the eight field campaigns ~~were compared directly (~~was presented in Fig. 5a~~).~~. It is ~~evident~~apparent that the ~~average~~ O/C ratios ~~of OAs were generally close to or larger than 1.0~~ at the remote sites of QOMS, Motuo, NamCo, Ngari, Waliguan, and LHG~~, whereas~~ typically reached or exceeded 1.0, indicating highly oxidized OA. In contrast, Bayanbulak exhibited a lower O/C ratio of 0.69 ~~was observed at Bayanbulak and~~, and the urban site of Lhasa showed an even lower ~~O/C~~ ratio of 0.44 ~~was observed at the urban site in Lhasa.~~. These variations in O/C ratios across sites primarily reflect differences in ~~O/C ratios were mainly attributed to the variations in~~ OA sources and aging processes ~~across different sites. As mentioned earlier, atmospheric aerosols in the remote~~. Remote sites in the TP were generally ~~associated with~~received well-mixed and aged OA due to long-range transport ~~from surrounding areas, hence the OAs were generally well-mixed and highly aged during the transport from source region to the remote sites in the TP~~ (Xu et al., 2018; Zhang et al., 2018; Zhang et al., 2019). ~~However~~Meanwhile, local ~~fresh OAs~~

625 ~~emitted~~emissions from ~~various residential~~ activities ~~such as~~like cooking, traffic
626 ~~exhausts~~, and biomass burning ~~predominated~~significantly contribute to the ~~total~~ OA ~~at~~in
627 urban Lhasa, resulting in a comparatively low O/C ratio (Zhao et al., 2022)~~, which~~
628 ~~ultimately led to a relatively low O/C ratio. Similar differences in O/C ratios have been~~.
629 This pattern of higher O/C ratios at remote sites and lower ratios at urban sites were
630 observed in previous ~~studies in~~findings across China. ~~For instance, higher~~, such as O/C
631 ratios of 0.98, 1.11, and 1.16 ~~were measured at remote sites in~~observed at Mt. Wuzhi
632 (Zhu et al., 2016), Mt. Yulong (Zheng et al., 2017), and LHG (Xu et al., 2015),
633 ~~while~~respectively, versus urban sites where O/C ratios ~~of OAs were generally lower~~
634 ~~than~~typically fell below 0.5 at most urban sites (Zhou et al., 2020). The Van Krevelen
635 diagram ~~(~~, which plots H/C versus O/C~~), a widely used approach~~ ratios to ~~depict~~
636 ~~the~~illustrate changes in ~~the~~OA elemental composition ~~of OA resulting from~~ due to
637 atmospheric aging ~~processing, is displayed in Fig. 5b. An~~, shows an overall slope of
638 −0.66 ~~was observed~~ for the bulk ~~OAs~~OA across ~~the eight field measurement~~all
639 campaigns ~~in our study, which~~. This result is comparable to ~~those~~slopes of −0.58 and
640 −0.47 obtained ~~from different synthesized datasets from diverse field observations~~ in
641 previous studies, further illustrating common pathways in OA aging (Chen et al., 2015;
642 Zhou et al., 2020).

643 The average HRMSs of OA between the remote site (Waliguan) and the urban site
644 (Lhasa) were directly compared to investigate the ~~inherent~~ difference in ~~ion~~ionic
645 compositions (Fig. 5c). Waliguan was ~~chosen as an example because the~~selected for
646 comparison due to its representation of overall highly~~-~~ aged OA~~nature~~, a characteristic
647 shared with ~~very similar HRMSs among the seven~~other remote sites~~, as shown in~~ (Fig.
648 S3 ~~in the supplementary materials. It is evident that the~~). The HRMS of OA ~~HRMSs~~
649 ~~exhibited distinct variations between these two types of sites. At the~~at Waliguan ~~site,~~
650 ~~and Lhasa displayed significant differences. At Waliguan, the~~ m/z 44, ~~which~~
651 ~~is~~predominantly composed ~~totally by~~of CO_2^+ and ~~one of the most reliable markers~~a
652 key marker for OOA, was the ~~base~~most prominent peak (18%) in the OA HRMS. The
653 CO_2^+ and its related ~~four~~ ions (CO^+, H_2O^+, HO^+ and O^+) together contributed ~~more~~
654 ~~than~~over 41% of the total OA signals. Additionally, ~~the~~ two oxygenated ion fragments
655 ($C_xH_yO_1^+$ and $C_xH_yO_2^+$) accounted for as much as 66% of the total OA signals (Fig.
656 5c~~). All these features demonstrated~~), suggesting the ~~overall~~ highly oxygenated nature
657 of OA at ~~the~~this remote ~~background sites in the TP.~~site. In contrast, the OA HRMS at

Lhasa was remarkably similar to those observed ~~at most~~in urban ~~cities.~~ ~~The~~environments, with significant contributions from four *m*/~~zs value~~*z* values at 43, 55, 57, and 60~~, which~~. These ions are recognized as ~~important mass spectral tracers~~markers for less oxidized OA ~~compounds~~ or primary emissions related to traffic, cooking, and biomass burning ~~activities~~ (Zhang et al., 2005a; Alfarra et al., 2007; He et al., 2010), ~~showed~~making up a significant ~~contributions~~contribution to the ~~total~~ OA signals in ~~this urban site.~~Lhasa. Specifically, ~~the~~non-oxygenated ion ~~fragment of~~ $C_x$fragments ($C_xH_y^+$) contributed as ~~higher~~much as 64.5% of the total OA ~~signal~~ in Lhasa, whereas the ~~two~~ oxygenated ~~ion~~ fragments ~~contributed~~accounted for only 33.6%. ~~The high contribution~~This pattern of fresh ion fragments in the OA HRMS in Lhasa is comparable to those measured at other urban cities, such as 56% and 59% in Lanzhou (Xu et al., 2014b; Xu et al., 2016), 51.2% in Nanjing (Wang et al., 2016), and 51.2% in New York (Sun et al., 2011).

4.4 OA components from PMF source apportionment

Source apportionments of OA were performed using PMF analysis on OA HRMS data for each field campaign. Figure 6 presents the average mass contributions of ~~different~~ OA components from the selected 2−4 factor solutions ~~among the~~across eight ~~different~~ field campaigns, while Figure S4 details the specific HRMS ~~of~~signatures for each OA component ~~is displayed in Fig. S4. Due to the~~. In regions with limited local ~~sources~~emissions but ~~dominated sources~~significant influence from regional transport, ~~only~~such as NamCo, LHG, and Bayanbulak, two secondary ~~OOA~~OA factors with different oxidation degrees, namely a less oxidized OOA (LO-OOA) and a more oxidized OOA (MO-OOA), were identified ~~during the NamCo, LHG, and Bayanbulak campaigns. On average~~. For instance, during the NamCo campaign, the MO-OOA and LO-OOA accounted for 59.0% and 41.0% of the total OA mass, with average O/C ratios of 0.96 and 0.49, respectively~~, accounted for 59.0% and 41.0% of the total OA mass. Similarly, the~~. The Bayanbulak campaign exhibited ~~contributions of~~a similar result, with MO-OOA (average O/C of 1.12) and LO-OOA (average O/C of 0.55) ~~to total OA mass at~~accounting for 66.3% and 33.7~~%,~~% of the OA mass, respectively. ~~However~~Contrastingly, the LHG campaign ~~showed only~~revealed a different pattern, with 24.9% ~~of~~MO-OOA and 75.1% ~~of~~LO-OOA, albeit with ~~relatively high~~higher O/C ratios of 1.29 and 1.08, respectively. ~~Besides~~Note that the ~~two~~properties of each OOA ~~factors~~factor could be different across the locations in the TP despite the same name.

Additionally, biomass-burning-related OA (BBOA) was also a prevalent component in the TP. At QOMS, the OA was composed by 42.4% MO-OOA, 43.9% BBOA, and 13.9% nitrogen-containing OA (NOA), with average O/C ratios of 1.34, 0.85, and 1.10, respectively. The high O/C ratio and significant contributions of BBOA and NOA at QOMS were linked to biomass burning emissions transported from South Asia during the pre-monsoon season (Cong et al., 2015; Zhang et al., 2018; Kang et al., 2019a). At Waliguan, the OA was composed by 34.4% MO-OOA, 40.4% relatively aged BBOA (agBBOA), 18.3% BBOA, and 6.9% hydrocarbon-like OA (HOA), with average O/C ratios of 1.42, 1.02, 0.69, and 0.33, respectively. The agBBOA exhibited an enhanced contribution to OA as the OA mass concentration increased, ranging from ~10% to 70% when OA mass varied from <1.0 µg m^{-3} to 7 µg m^{-3} (Zhang et al., 2019). High contributions of BBOA at Waliguan were associated with regional transport of biomass burning emissions from areas in the northeast (Zhang et al., 2019). At Ngari, the OA was composed by 43.7% MO-OOA, 28.5% LO-OOA, and 27.8% BBOA, with average O/C ratios of 1.43, 1.00, and 0.56, respectively. In contrast, Motuo exhibited OA components of 36.9% MO-OOA, 46.9% LO-OOA, and 16.2% BBOA, with O/C ratios of 1.30, 1.11, and 0.25, respectively. The lower BBOA contribution and O/C ratio at Motuo suggest a weaker local biomass burning emissions. At urban Lhasa, four OA factors were identified including an OOA with O/C ratio of 0.54 and three primary OA components, i.e., BBOA (O/C of 0.13), cooking-related OA (COA, O/C of 0.12), and HOA (O/C of 0.11). These components were markedly different from those at above remote sites with the three primary OA components accounting for more than 60% of the total OA, suggesting the abundant primary aerosol sources from the residential activities. In addition, the BBOA contribution increased significantly (up to 36%) during a major local festival in Lhasa, suggesting the crucial aerosol source from biomass burning during

725 religious activities in the city (Zhao et al., 2022). ~~In summary, distinct types of OA~~
726 ~~components with different O/C ratios were identified at different sites, indicating the~~
727 ~~different sources and oxidation states of OA in the different TP regions.~~
728 In summary, our study identified diverse OA components with varying O/C ratios at
729 different sites, indicating the heterogeneity of sources and oxidation states of OA across
730 the TP regions.

4.5 Number concentrations of submicron aerosols and cloud condensation nuclei

732 ~~Real-time online measurements of the size distribution of number concentration of fine~~
733 ~~particles were also conducted simultaneously using SMPS instruments during four field~~
734 ~~campaigns (QOMS, Motuo, LHG, and Lhasa).~~ The measurement of particle number
735 size distribution (PNSD) was ~~not only an important auxiliary data for calibrating and~~
736 ~~verifying the accuracy of HR-ToF-AMS data, but also very~~ useful for studying the
737 formation and growth mechanisms of aerosol particles in the atmosphere. Figure 7a
738 shows the high-resolution temporal variations of the PNSDs during ~~the~~ four field
739 campaigns. ~~The PNSDs varied dynamically throughout the measurement period at each~~
740 ~~site and showed distinct variations in~~ (QOMS, Motuo, LHG, and Lhasa), revealing
741 significant variability in number concentrations and size distribution ~~pattern~~
742 ~~among~~patterns across the ~~four~~ different ~~campaigns~~sites. On average, the total number
743 ~~concentrations were~~concentration was 709.3 and 3994.4 cm^{-3} at QOMS and Lhasa,
744 respectively, while ~~they were~~it was 1639.2 and 1462.0 cm^{-3} at Motuo and LHG.
745 ~~Interestingly~~Notably, the ~~difference~~variations in particle number concentrations were
746 not consistent with ~~those in~~ mass concentrations measured from the HR-ToF-AMS
747 ~~among~~at the four ~~campaigns~~sites (Table 2). For ~~example~~instance, although the PM$_1$
748 mass concentration at Lhasa was comparable to that at QOMS (4.7 versus 4.4 μg m^{-3}),
749 the number concentration at Lhasa was more than five times higher than that at QOMS.
750 This inconsistency ~~may be~~was mainly related to the ~~distinctly different~~difference on
751 size distribution at different sites. As ~~discussed~~mentioned above, submicron aerosols at
752 QOMS were ~~overall highly aged~~predominantly secondary due to ~~the~~ long-range
753 ~~transported sources~~transport from South Asia and ~~dominated~~characterized by ~~aerosols~~
754 ~~at~~ accumulation mode ~~size~~ ~~mode, whereas more fresh.~~ In contrast, Lhasa exhibited
755 fresher aerosols, emitted from local residential activities and ~~dominated~~characterized
756 by ~~aerosols of~~ Aitken ~~size~~ mode ~~were observed at Lhasa.~~size. The ~~different sizes of~~
757 variation in submicron ~~aerosols among~~aerosol sizes across the ~~different~~ TP ~~regions~~

~~could be~~was further ~~confirmed~~evidenced by the peak diameters in the average mass and number size distributions ~~of mass and number concentrations~~ (Figs. 4a and 7b). For ~~example~~instance, the average OA mass size ~~distributions exhibited peak diameters of distribution~~ peaked at 510.2 and 430.5 nm in D_{va} ~~at~~for QOMS and Motuo, respectively~~, while~~. Meanwhile, the average number size distributions at these two sites had peak ~~diameters of~~at 109.4 and 131.0 nm in D_m ~~at the same sites.~~. In contrast, Lhasa displayed significantly smaller peak diameters of only 228.1 nm in D_{va} and 28.9 nm in D_m.

New particle formation (NPF) events were ~~also~~ observed at ~~a few~~several sites in our study. Typically, an NPF event is characterized by a rapid burst in nucleation mode followed by the subsequent growth into larger particles, as defined as banana-shaped temporal developments in the PNSD (Dal Maso et al., 2005). ~~As shown in Fig.~~Figure 7a~~, frequent~~ displays the cases of banana-shaped ~~variation~~patterns in the PNSD, which were frequently observed at ~~Lhasa, suggesting the frequent occurrence of NPF at this~~urban ~~region. During~~Lhasa. Throughout the 27-day Lhasa campaign ~~(27 days),~~, a total of 10 NPF events were observed (Zhao et al., 2022). In contrast, ~~this~~such banana-shaped pattern in the PNSD was relatively rare at the other three remote sites~~,~~ (QOMS, Motuo, and LHG), which might be related to their ~~predominated transport~~predominance of long-range transported aerosol ~~sources,~~with overall highly-aged states~~,~~ and limited gaseous precursors.

Cloud condensation nuclei (CCN) is a distinct class of atmospheric aerosol particles which could be activated as cloud droplets at a certain supersaturated water vapor condition and played important roles in cloud formation, ~~atmospheric~~ precipitation, ~~the~~climate change, and regional ~~climate, as well as the~~ hydrological cycle (Andreae and Rosenfeld, 2008). ~~During~~Across the TP field campaigns, ~~real-time online~~ CCN measurements ~~of CCN number concentrations~~ were conducted at three sites~~, i.e.,~~: Motuo ~~in the southeastern TP while~~, Waliguan, and LHG ~~in the northeastern TP. Generally, the~~. The temporal ~~variation~~variations of CCN number ~~concentration~~concentrations at each SS exhibited a ~~consistent~~similar trend with the total number concentration from the SMPS measurement ~~or total~~and the PM_1 mass concentration from the HR-ToF-AMS measurement during each campaign. On average, ~~at Motuo,~~the CCN number concentrations at Motuo were 974.0, 1142.6, 1240.1, 1296.5, and 1337.9 cm^{-3} at ~~different~~ SS ~~values~~level of 0.2%, 0.4%, 0.6%, 0.8%, and 1.0%, respectively. At Waliguan, relatively comparable average values of ~~507.0, 805~~233.7,

857.8, 1138.7, 1313.1, ~~1073.3, 1230.6,~~ and ~~1336.6~~1407.0 cm^{-3} were observed at ~~the~~ ~~same SS steps, respectively. However, at~~corresponding SS levels. In contrast, LHG~~,~~ ~~these average values~~ exhibited significantly ~~decreased to 83.9, 344.3, 429.9, 480.8,~~ lower average CCN concentration of 120.5, 340.1, 417.8, 468.0, and ~~516.1~~504.5 cm^{-3} at the same *SS* levels, respectively (Table 2). The lower CCN number concentrations at LHG compared to Waliguan and Motuo were consistent with ~~the relatively~~its lower PM$_1$ mass loading ~~at the LHG site. The~~. Comparing with other regions, the CCN number concentrations at the three TP sites were almost an order of magnitude lower than those observed in polluted urban ~~atmospheres~~environments or ~~emissions of~~from specific combustion ~~sources, such as~~emissions. For instance, CCN concentrations reached 12963 cm^{-3} (*SS* = 0.70%) in Wuqing, 9890 cm^{-3} (*SS* = 0.86%) in Beijing (Deng et al., 2011; Gunthe et al., 2011), 7913 cm^{-3} (*SS* = 0.70%) at Panyu in the Pearl River Delta, as well as 11565 cm^{-3} (*SS* = 0.87%) and 10000 cm^{-3} (*SS* = 0.80%) during unique biomass burning plumes (Rose et al., 2010; Zhang et al., 2020). However, ~~our~~the CCN values from our study were comparable to those ~~(228−2150 cm^{-3} with SS of 0.87%)~~ measured at eight remote marine sites in the South China Sea (228−2150 cm^{-3} at *SS* = 0.87%) and ~~941 cm^{-3} (SS = 0.74%) in~~the amazon rain forest (941 cm^{-3} at *SS* = 0.74%) (Pöhlker et al., 2016; Atwood et al., 2017). These comparisons again highlight the overall clean atmospheric condition in the TP.

4.6 Aerosol optical properties and light absorptions from BC and BrC

~~The optical properties of aerosol particles are crucial input parameters for accurately~~ ~~estimating aerosol radiative forcing in climate models. However, significant~~ ~~uncertainties persist due to the limited dataset in~~ In this ~~remote region. In our~~ ~~project~~study, the parameters of B_{scat}, B_{abs}, and SSA of fine particles at 405 nm were observed ~~during five~~at the field campaigns~~, i.e.,~~ of QOMS, Motuo, Waliguan, Ngari, and Lhasa, to explore the ~~differences~~variations in aerosol optical properties ~~at~~ ~~different~~across the TP ~~regions~~. On average, the B_{scat} and B_{abs} at 405 nm during the five campaigns were 121.9, 44.9, 36.3, 8.9, and 2.1 Mm^{-1} and 10.8, 7.0, 4.1, 3.6, and 1.9 Mm^{-1}, respectively~~, which finally resulted in~~. These values yielded average SSA values of 0.89, 0.83, 0.86, 0.67, and 0.52, correspondingly (Fig. 8a and Table 2). ~~These~~The B_{scat} and B_{abs} values at the ~~five~~TP sites were ~~both~~significantly lower than those reported ~~at~~in various urban ~~sites~~areas in China, such as 459.5 and 47.2 Mm^{-1}~~, respectively,~~ at 630 nm in Beijing (Xie et al., 2019), 272 and 31 Mm^{-1}~~, respectively,~~ at 532 nm in Xi'an

(Zhu et al., 2015), and 418 and 91 Mm^{-1}, respectively, at 540 nm in Guangzhou (Andreae et al., 2008), once again suggesting the overall clean atmospheric condition in the TP. Although the PM$_1$ mass concentrations at QOMS was comparable to or even lower than those at the other four sites, QOMS exhibited the highest B_{scat}, B_{abs}, and SSA values were observed at QOMS. These results. This discrepancy may be attributeddue to the differencesvariations in aerosol chemical compositions and their mass scattering and absorbing efficiencies. In contrast, Lhasa exhibited a significantly lower SSA compared to the other four remote sites, suggesting a prevalence of fresh aerosols in the urban areaenvironment. On the other hand, aerosols at the four remote sites were highly aged, which resulted in leading to significant photobleaching inof BrC chromophores and an obvious decrease in their light absorptivity at these sites.

In this study, realReal-time online measurements of particle B_{abs} at seven fixed wavelengths (ranging from 370= to 950 nm) were also conducted using an aethalometer at QOMS, NamCo, and Waliguan, respectively, to explore the regional differencevariations in aerosol absorption properties inacross the different TP regions. Overall, the muti-wavelength B_{abs} decreased significantly with the increasing wavelength during all the three measurement campaigns, with fittingfitted AAE values to beof 1.73, 1.28, and 1.12, respectively (Fig. 8b). The average B_{abs} at the shortest wavelength of 370 nm was 13.40, 3.25, and 2.66 Mm^{-1} at the three sites, respectively (Table 2). AlthoughDespite a relatively low PM$_1$ mass was observedconcentrations at QOMS, the B_{abs} at 370 nm was five times higher than that at Waliguan, mainly asdue to a result of the higher contribution of light-absorbing aerosol components in the southern TP regions. For example. Specifically, OA and BC together contributedaccounted for nearly 80% of the total PM$_1$ at QOMS, whereas this contribution decreased to only 37.5% at Waliguan. The obviously higher AAE at QOMS also suggested a dominant light-absorbing contribution from BrC or the significant lensing effect of non-BC materials coated on BC at this southern siteBC (Zhang et al., 2021). As shown in theThe inserted plots in Fig. 8b, both BC and BrC components showed illustrate significant decrease ofdecreases in particle B_{abs} ($_{BC}$ and $B_{abs,BC}$ and$_{BrC}$ to total $B_{abs,BrC}$) with increasing wavelength, butyet their contributions to total B_{abs} ($fB_{abs,BC}$ and $fB_{abs,BrC}$) varied inversely. BC was the primary light-absorbing component atacross all the three sites, contributing 66.9%, 78.7%, and 77.6% to the total B_{abs} at 370 nm at QOMS, NamCo, and Waliguan sites, respectively, and; its

857 contribution increased apparently with longer wavelengths (Table 2). Conversely, BrC

858 showed more significant contributions to total B_{abs} at shorter wavelengths. For

859 ~~example~~instance, the average $B_{abs,BrC}$ at 370 nm were 4.42, 0.69, and 0.60 Mm^{-1} at the

860 three sites, respectively, ~~which finally contributed~~ultimately contributing 33.1%, 21.3%,

861 and 22.4% ~~of~~to the total B_{abs}. The significantly higher values of total B_{abs}, $B_{abs,BC}$,

862 $B_{abs,BrC}$, and $fB_{abs,BrC}$ in the southern TP region could be related to the important

863 contributions of light-absorbing CAs from transported biomass burning emissions (Xu

864 et al., 2020, 2022).

4.7 Estimation of aerosol radiative forcing in the different TP regions

866 Atmospheric aerosols ~~have been found to significantly impact the~~play a significant role

867 in impacting Earth's climate systems through affecting solar radiation and exerting a

868 positive forcing on the energy budget (Bond and Bergstrom, 2006). In this study,

869 aerosol direct radiative forcings (DRF) caused by BC, organic carbon (OC), and water-

870 soluble ions (WSIs) are estimated, respectively, ~~by the widely used~~using Santa Barbara

871 DISORT (Discrete Ordinate Radiative Transfer) Atmospheric Radiative Transfer

872 (SBDART) model (Ricchiazzi et al., 1998). A detailed introduction and operation

873 ~~process~~ of this model are described in Text S6 in the supplementary material. Since the

874 model's performance is evaluated and calibrated by comparing the values with

875 measurements from ~~the~~ Aethalometer and PAX ~~instruments~~results, the aerosol DRF

876 estimations are limited to ~~the three sites of~~ QOMS, NamCo, and Waliguan~~, which have~~

877 ~~both online measurements from the aforementioned instruments~~. Furthermore, these

878 three sites are located in the southern, central, and northern regions of the TP,

879 respectively, which ~~enables us to explore the~~allows for an exploration of regional

880 variations in aerosol DRF across ~~different~~the TP~~regions~~.

881 Figure 9 presents the ~~modelled~~results of DRFs ~~caused by~~attributed to BC, OC, and

882 WSIs ~~during~~across the three campaigns. BC ~~exhibited~~demonstrated a

883 ~~significant~~pronounced warming effect at the top of the atmosphere, with average DRF

884 values of +2.5 ± 0.5, +2.1 ± 0.1, and +1.9 ± 0.1 $W\ m^{-2}$ during the QOMS, Waliguan,

885 and NamCo ~~campaign~~campaigns, respectively. In contrast, BC exhibited a noticeable

886 cooling effect ~~caused by BC was observed~~ at the earth's surface, with average DRF

887 values of −4.7 ± 0.8, −4.1 ± 0.2, and −3.7 ± 0.1 $W\ m^{-2}$ across the three campaigns. The

888 combination of ~~warming effect at the top of the atmosphere and cooling effect at the~~

889 ~~earth's surface~~ these two effects resulted in significantly high net atmospheric

~~forcings~~forcing by BC, amounting to +7.3 ± 1.2, +6.2 ± 0.3, and +5.6 ± 0.2 W m^{-2} ~~during~~for the ~~QOMS, Waliguan, and NamCo~~three campaigns~~, respectively.~~. These ~~findings~~results suggest the important radiative effect ~~caused by~~of BC in the TP, especially in the southern ~~TP~~region~~, which was significantly~~ influenced by ~~the~~ long-range transported biomass burning emission from South Asia. ~~For~~In contrast, OC and WSIs~~,~~ exhibited cooling effects ~~were observed~~ at both the top of the atmosphere and the ~~earth's~~Earth's surface, characterized by negative and relatively low average DRFs. Consequently, the net atmospheric forcings for OC and WSIs were ~~significantly~~notably lower compared to BC across the three campaigns, with values of +2.0 ± 1.2, +0.7 ± 0.2, and +0.9 ± 0.7 W m^{-2} for OC, and +1.9 ± 0.8, +1.4 ± 0.6, and +1.2 ± 0.2 W m^{-2} for WSIs at QOMS, Waliguan and NamCo, respectively. Interestingly, at QOMS, the average atmospheric DRF of OC accounted for 27.3% of that of BC, whereas at Waliguan and NamCo, the fractions were only 11.1% and 15.7%, respectively. The higher atmospheric DRF observed at QOMS suggests a dominant contribution from light-absorbing BC and BrC aerosols~~,~~ compared to Waliguan and NamCo.

It was worth noting that the simulations of DRF effects in this study were only conducted at three specific sites ~~during~~over limited periods. ~~Therefore,~~Future research should focus on long-term comprehensive measurements and DRF simulations ~~over~~across the entire TP ~~regions under different seasons are needed in the future~~to enhance our understanding of aerosol impacts on regional climate.

4.8 Long-range transport of aerosols from surrounding areas

To further understand the potential sources and specific transport pathways of ~~air masses~~aerosols at each site, particularly for those remote sites ~~where regional transport dominated~~, three- or five-days air mass back trajectories were calculated during each measurement period at an ending height of 500 m above ground level every 6h using the Hybrid Single Particle Lagrangian Integrated Trajectory (HYSPLIT) model (Draxler and Rolph, 2003). The cluster analysis on the trajectories was based on the total spatial minimum variance method. Figure 10 ~~display~~displays the average backward trajectory clusters ~~during~~across all ~~the~~ eight field campaigns ~~and the major trajectory clusters at each site are marked with large solid circles in different colors~~.

In general, distinct air mass sources were identified ~~among~~across the ~~different~~ TP ~~regions~~. The five sites (QOMS, Motuo, Lhasa, NamCo, and Ngari) located in the

southern or south-central part of the TP generally showed air masses from south or southwest with different transport distances and pathways during their measurement periods. For instance, during the QOMS campaign, 38% of the air masses originated from the west, covering a long distance, while another 40% originated from the southwest, covering a shorter distance. In the Motuo campaign, two major clusters both originated from the southwest with different distances (77% at shorter distance compared to only 13% at a longer distance). Similarly, during the NamCo campaign, two major clusters with comparable contributions (37% and 34%) and transport distances but different pathways were identified from the south. In the Ngari campaign, air masses showed similar transport distances, with 56% originating from southwest and 26% from the south. These air mass clusters originating from the south of the TP generally traverse polluted regions in South Asia such as the Indo-Gangetic Plain, Nepal, and Bangladesh, carrying significant amounts of pollutants, particularly biomass-burning emissions into the inland of the TP. In contrast, air masses at northern sites were primarily influenced by Westerlies and East Asian monsoon during summer season. In the campaigns of Bayanbulak, air masses originated from the west with different distances, i.e., 69% in relatively shorter distance versus 18% in a longer distance. During the LHG campaign, the air masses originated from the northwest of the site with 63% in longer distance but 27% in shorter distance. For the Waliguan campaign, the air mass originated from two distinct directions. Most of the air masses (57%) came from the northeast of the site with a shorter distance, while the remaining air masses originated from the west and northwest with longer distances.

In summary, significant variations in air mass sources and transport pathways were observed across the TP, particularly between southern and northern regions. These differences play a crucial role in shaping the different

955   physiochemical and optical properties of aerosols ~~in~~across the ~~different~~ TP regions.

5 Dataset limitations and applications

957   Our dataset was ~~achieved~~compiled from ~~multiple~~eight short-term intensive field
958   observations ~~conducted at eight different sites of~~across the TP ~~during their high mass~~
959   ~~loading periods~~ utilizing a suite of high-resolution online instruments. However, it is
960   important to ~~acknowledge~~note that our dataset ~~has~~does have certain limitations ~~due to~~
961   ~~objective restrictions~~ that ~~were~~proved to be quite challenging to ~~overcome~~address in
962   these remote regions.

963   The primary limitation ~~revolves around~~stems from the short and inconsistent
964   measurement periods across different observational years and seasons at different sites~~.~~
965   ~~This limitation hinders the ability to make a~~, impeding robust ~~comparison~~comparisons
966   of aerosol properties across the ~~vast TP region,~~TP. This limitation also hampers the
967   ability to ascertain long-term and seasonal ~~variation~~characteristics~~, and apply the~~
968   ~~current data and findings to other different seasons.~~. The harsh natural environments,
969   challenging weather conditions, limited logistical support~~, sole availability of our high~~
970   ~~resolution~~ and instruments, and ~~the~~stringent instrumental requirements (~~e.g.,~~such as
971   the ~~need~~necessity for comprehensive field stations with ~~uninterrupted and~~stable power
972   supply) ~~were the most~~presented significant challenges ~~we faced~~ during our field
973   observations in these remote TP regions. It is worth noting that online HR-ToF-AMS
974   observations, such as the ~~ones~~one we conducted, are predominantly short-term and
975   ~~intense~~intensive observations carried out worldwide due to the ~~stability~~instability issues
976   and its challenging maintenance ~~during~~required for long-term
977   ~~measurement~~measurements. The short-term intensive measurement ~~can well~~is enough
978   to capture and characterize the dynamic evolution of aerosol properties at a high-time-
979   resolution (Jimenez et al., 2009; Li et al., 2017). ~~Until now, long~~Long-term high-time-
980   resolution observation utilizing HR-ToF-AMS have been rarely ~~been~~conducted thus
981   far, even ~~at~~in urban ~~sites~~environment with relatively favorable observational
982   ~~environments~~conditions and logistic support compared to our remote TP sites.
983   Consequently, performing continuous long-term observations or simultaneous
984   comparison at multiple sites in these high-altitude remote ~~and challenging TP regions,~~
985   ~~without stable power supply, is nearly impossible~~TP regions, without stable power
986   supply, is exceedingly challenging. Furthermore, assessing the representativeness of
987   each observation for the spatial scale is particularly challenging due to the limited

number of observatories across the TP. Actually, these observatories have been strategically established based on the representation of specific geographic and climatic features.

~~However~~In addition to the limitations above, our team has made significant efforts to conduct ~~the~~this comprehensive observation project over the past ~~ten years~~decade, aiming to study the regional differences in aerosol sources and properties across the ~~different~~ TP ~~regions~~. The dataset generated from our project represents the first and ~~sole~~exclusive high-time-resolution dataset focusing on atmospheric aerosol physicochemical and optical properties, ~~coring the~~covering most ~~part~~region of the TP. The applications of this dataset in atmospheric science ~~can be summarized as follows: firstly~~are multifaceted. Firstly, the high-time-resolution observations offer crucial advantages in understanding the rapid evolution and diurnal variations of aerosol properties during a short period or special event. ~~Additionally~~Furthermore, these observations are ~~valuable~~invaluable for model simulation and verification, ~~as they provide sufficient~~providing a wealth of data points~~.~~ that can be utilized for assessing aerosol loading, chemical composition, size distribution, and other parameters essential for model accuracy and validation. Such advantages are not achievable with traditional off-line samplings, which ~~have~~typically exhibit low time resolutions ranging from days to weeks. Secondly, the eight sites ~~included~~encompassed in our project effectively represent a wide range of the TP. This is particularly noteworthy considering the limited availability of ~~observational stations~~observatories on the ~~plateau. Furthermore, these~~TP. These sites ~~provide excellent opportunities for comparing~~facilitate comparisons of aerosol sources and properties among different ~~types of sites with varying altitudes, land covers, surrounding environments, human activities, and influences from large-scale atmospheric circulations~~regions. Thirdly, our observations encompass a wide range of aerosol physical, chemical, and optical parameters, including aerosol mass loadings, chemical compositions, size distribution, diurnal variations, number concentrations, light scattering and absorption coefficients, and so on. This comprehensive dataset ~~is~~plays a crucial ~~for a thorough~~role in fostering a profound understanding of aerosol properties in the TP ~~regions. Overall, it is worth noting that until now, similar online observational aerosol datasets focusing on multiple parameters with at least hourly-scale resolution at various sites in the diverse TP regions had been rarely reported..~~

Overall, it is noteworthy that our online observational aerosol datasets, focusing on multiple parameters with at least hourly-scale resolution at various sites across the TP, are the only ones reported to date.

6 Data availability

The high-resolution online measurement datasets, encompassing aerosol physical, chemical, and optical properties over the Tibetan Plateau and its surroundings in our observation project have been released and are now available for download from the National Cryosphere Desert Data Center (https://doi.org/10.12072/ncdc.NIEER.db2200.2022). These datasets are provided in an Excel file comprising eight worksheets. The first sheet of the Excel file contains a concise description of the dataset, including the dataset name, observation stations, sampling periods, online instruments used, and corresponding references. The remaining seven sheets present the high-resolution measurement data obtained from the online instruments employed during the eight campaigns. These instruments include HR-ToF-AMS, SMPS, PAX, aethalometer, and CCN-100.

7 Conclusions

AThis study presents a comprehensive dataset includingencompassing aerosol physicochemical and optical properties, especially thewith a particular focus on high-resolution size-resolved chemical characteristics and sources of submicron aerosols, conducted through real-time online measurements at at eight different sites of the TP and its surroundings is presented in this study.. The objective of this study is to elucidate the mass concentration level of atmospheric aerosols in this isolated background region and identify regional variations in aerosol sources, as well as physicochemical and optical properties among different TP regions. Ultimately, these valuable data will significantly contribute to accurately simulating the radiative forcing and other potential impacts of atmospheric aerosols in this remote region in future climatic models.

A total of eight aerosol field measurements were conducted at QOMS, Motuo, NamCo, Ngari, Waliguan, LHG, Bayanbulak, and Lhasa in the different regions of TP and its surroundings by deploying multiple online instruments, including HR-ToF-AMS, SMPS, PAX, Aethalometer, and CCN-100. The datasets collected datasets provide the offer insights into temporal and diurnal variations as well as the, size distribution

patterns of PM$_1$ chemical compositions, ~~the standard high-resolution mass spectra and temporal variations of OA~~HRMS and chemical components, ~~the temporal variations of particle number size distribution~~ of OA, particle light scattering and absorption coefficients, ~~particle light absorptions from different CAs of BC and BrC,~~ and CCN number concentrations at different ~~supersaturation in each campaign~~supersaturations in different campaigns.

The datasets ~~provide~~offer valuable insights into ~~the~~ regional variations in aerosol properties and sources. In the southern TP region, atmospheric aerosols were ~~found to be~~ primarily influenced by biomass burning emissions transported from ~~polluted regions in~~ South Asia, ~~which~~ resulted in high mass contributions (>70%) of CAs and overall neutralized PM$_1$, as well as an enhanced light absorption capability of ~~the light-absorbing BC and BrC.~~aerosols. In contrast, in the northern TP, secondary inorganic species, particularly sulfate, contributed significantly to total PM$_1$ due to the regional transport of anthropogenic aerosol and gaseous precursor emissions from urban areas in northwestern China. Furthermore, in contrast to the well-mixed, highly-aged, and regionally transported aerosols observed in the remote sites, atmospheric aerosols in the urban Lhasa were mainly originated from local primary sources such as cooking, traffic vehicle exhausts, and biofuel combustion during the residential activities. Consequently, these aerosol particles were relatively fresh, characterized by small size and low oxidation degree, but exhibited a high frequency of NPF origins.

Appendix A: Main Abbreviations

TP	Tibetan Plateau
HR-ToF-AMS	high-resolution time-of-flight aerosol mass spectrometer
SMPS	scanning mobility particle sizer
PAX	photo-acoustic extinctiometer
CCN	cloud condensation nuclei
SS	supersaturation
PM$_1$	submicron aerosol
BC	black carbon
BrC	brown carbon
OA	organic aerosol
SNA	sulfate, nitrate, and ammonium
D_m	mobility diameter
D_{va}	aerodynamic diameter
CE	collection efficiency
HRMS	high-resolution mass spectrum
PBL	planetary boundary layer
O/C	oxygen-to-carbon ratio

H/C	hydrogen-to-carbon ratio
N/C	nitrogen-to-carbon ratio
OM/OC	organic matter-to-organic carbon ratio
PMF	positive matrix factorization
OOA	oxygenated organic aerosol
LO-OOA	less oxidized oxygenated organic aerosol
MO-OOA	more oxidized oxygenated organic aerosol
BBOA	biomass-burning-related organic aerosol
agBBOA	aged biomass-burning-related organic aerosol
NOA	nitrogen-containing organic aerosol
HOA	traffic-related hydrocarbon-like organic aerosol
COA	cooking-related organic aerosol
PNSD	particle number size distribution
NPF	new particle formation
B_{scat}	light scattering coefficient
B_{abs}	light absorption coefficient
B_{ext}	light extinction coefficient
SSA	single scattering albedo
AAE	absorption Ångström exponents
$B_{abs,BC}$	light absorption coefficient from BC
$B_{abs,BrC}$	light absorption coefficient from BrC
OC	organic carbon
WSIs	water-soluble ions
DRF	direct radiative forcing

Author Contributions. JX designed the study, XZ, WZ, and JX wrote the manuscript. JX and SK organized and supervised the field measurement campaigns, JX, XZ, WZ, LZ, MZ, JS, JShi, YL, CX, YT, KL, XG, and QZ conducted the field measurements, JX, XZ, WZ, and YT analyzed the data. All authors reviewed and commented on the final form of the manuscript.

Competing interests. The authors declared that they have no competing interests.

Acknowledgements. We ~~appreciate~~extend our thanks to all our colleagues and collaborators who participated the aerosol field measurements, maintained the instruments, analyzed the data, and commented on the manuscript. We also show great thanks to all the observation stations in this study for their logistical supports with the field campaigns.

Financial support. This work was supported by the National Natural Science Foundation of China (41977189, 41771079, 41805106), the Second Tibetan Plateau Scientific Expedition and Research program (STEP) (2019QZKK0605), the Strategic Priority Research Program of Chinese Academy of Sciences, Pan-Third Pole

Environment Study for a Green Silk Road (Pan-TPE) (XDA20040501), the State Key Laboratory of Cryospheric Sciences Scientific Research Foundation (SKLCS-ZZ-2023), and the Chinese Academy of Sciences Hundred Talents Program.

References

Aiken, A. C., Salcedo, D., Cubison, M. J., Huffman, J. A., DeCarlo, P. F., Ulbrich, I. M., Docherty, K. S., Sueper, D., Kimmel, J. R., Worsnop, D. R., Trimborn, A., Northway, M., Stone, E. A., Schauer, J. J., Volkamer, R. M., Fortner, E., de Foy, B., Wang, J., Laskin, A., Shutthanandan, V., Zheng, J., Zhang, R., Gaffney, J., Marley, N. A., Paredes-Miranda, G., Arnott, W. P., Molina, L. T., Sosa, G., and Jimenez, J. L.: Mexico City aerosol analysis during MILAGRO using high resolution aerosol mass spectrometry at the urban supersite (T0) – Part 1: Fine particle composition and organic source apportionment, Atmos. Chem. Phys., 9, 6633-6653, https://doi.org/10.5194/acp-9-6633-2009, 2009.

Alfarra, M. R., Prevot, A. S. H., Szidat, S., Sandradewi, J., Weimer, S., Lanz, V. A., Schreiber, D., Mohr, M., and Baltensperger, U.: Identification of the mass spectral signature of organic aerosols from wood burning emissions, Environ. Sci. Technol., 41, 5770-5777, https://doi.org/10.1021/es062289b, 2007.

An, Y., Xu, J., Feng, L., Zhang, X., Liu, Y., Kang, S., Jiang, B., and Liao, Y.: Molecular characterization of organic aerosol in the Himalayas: insight from ultra-high-resolution mass spectrometry, Atmos. Chem. Phys., 19, 1115-1128, https://doi.org/10.5194/acp-19-1115-2019, 2019.

Andreae, M. O., and Rosenfeld, D.: Aerosol–cloud–precipitation interactions. Part 1. The nature and sources of cloud-active aerosols, Earth-Science Reviews, 89, 13-41, https://doi.org/10.1016/j.earscirev.2008.03.001, 2008.

Andreae, M. O., Schmid, O., Yang, H., Chand, D., Zhen Yu, J., Zeng, L.-M., and Zhang, Y.-H.: Optical properties and chemical composition of the atmospheric aerosol in urban Guangzhou, China, Atmos. Environ., 42, 6335-6350, https://doi.org/10.1016/j.atmosenv.2008.01.030, 2008.

Atwood, S. A., Reid, J. S., Kreidenweis, S. M., Blake, D. R., Jonsson, H. H., Lagrosas, N. D., Xian, P., Reid, E. A., Sessions, W. R., and Simpas, J. B.: Size-resolved aerosol and cloud condensation nuclei (CCN) properties in the remote marine South China Sea – Part 1: Observations and source classification, Atmos. Chem. Phys., 17, 1105-1123, https://doi.org/10.5194/acp-17-1105-2017, 2017.

Backman, J., Schmeisser, L., Virkkula, A., Ogren, J. A., Asmi, E., Starkweather, S., Sharma, S., Eleftheriadis, K., Uttal, T., Jefferson, A., Bergin, M., Makshtas, A., Tunved, P., and Fiebig, M.: On Aethalometer measurement uncertainties and an instrument correction factor for the Arctic, Atmos. Meas. Tech., 10, 5039–5062, https://doi.org/10.5194/amt-10-5039-2017, 2017.

Bonasoni, P., Laj, P., Marinoni, A., Sprenger, M., Angelini, F., Arduini, J., Bonafè, U., Calzolari, F., Colombo, T., Decesari, S., Di Biagio, C., di Sarra, A. G., Evangelisti, F., Duchi, R., Facchini, M. C., Fuzzi, S., Gobbi, G. P., Maione, M., Panday, A., Roccato, F., Sellegri, K., Venzac, H., Verza, G. P., Villani, P., Vuillermoz, E., and Cristofanelli, P.: Atmospheric Brown Clouds in the Himalayas: first two years of continuous observations at the Nepal Climate Observatory-Pyramid (5079 m), Atmos. Chem. Phys., 10, 7515-7531, https://doi.org/10.5194/acp-10-7515-2010, 2010.

Bond, T. C., and Bergstrom, R. W.: Light absorption by carbonaceous particles: An investigative review, Aerosol Sci. Technol., 40, 27-67, https://doi.org/10.1080/02786820500421521, 2006.

Canagaratna, M. R., Jimenez, J. L., Kroll, J. H., Chen, Q., Kessler, S. H., Massoli, P., Hildebrandt Ruiz, L., Fortner, E., Williams, L. R., Wilson, K. R., Surratt, J. D., Donahue, N. M., Jayne, J. T., and Worsnop, D. R.: Elemental ratio measurements of organic compounds using aerosol mass spectrometry: characterization, improved calibration, and implications, Atmos. Chem. Phys., 15, 253-272, https://doi.org/10.5194/acp-15-253-2015, 2015.

Cao, J., Xu, B., He, J., Liu, X., Han, Y., Wang, G., and Zhu, C.: Concentrations, seasonal variations, and transport of carbonaceous aerosols at a remote Mountainous region in western China, Atmos. Environ., 43, 4444-4452, https://doi.org/10.1016/j.atmosenv.2009.06.023, 2009.

Chen, F., Ding, L., Piao, S., Zhou, T., Xu, B., Yao, T., and Li, X.: The Tibetan Plateau as the engine for Asian environmental change: the Tibetan Plateau Earth system research into a new era, Science Bulletin, 66, 1263-1266, https://doi.org/10.1016/j.scib.2021.04.017, 2021.

Chen, P., Kang, S., Li, C., Zhang, Q., Guo, J., Tripathee, L., Zhang, Y., Li, G., Gul, C., Cong, Z., Wan, X., Niu, H., Panday, A. K., Rupakheti, M., and Ji, Z.: Carbonaceous aerosol characteristics on the Third Pole: A primary study based on the Atmospheric Pollution and Cryospheric Change (APCC) network, Environ. Pollut., 253, 49-60, https://doi.org/10.1016/j.envpol.2019.06.112, 2019.

Chen, Q., Heald, C. L., Jimenez, J. L., Canagaratna, M. R., Zhang, Q., He, L. Y., Huang, X. F.,

Campuzano‑Jost, P., Palm, B. B., Poulain, L., Kuwata, M., Martin, S. T., Abbatt, J. P. D., Lee, A. K. Y., and Liggio, J.: Elemental composition of organic aerosol: The gap between ambient and laboratory measurements, Geophys. Res. Lett., 42, 4182-4189, https://doi.org/10.1002/2015gl063693, 2015.

Cong, Z., Kang, S., Kawamura, K., Liu, B., Wan, X., Wang, Z., Gao, S., and Fu, P.: Carbonaceous aerosols on the south edge of the Tibetan Plateau: concentrations, seasonality and sources, Atmos. Chem. Phys., 15, 1573-1584, https://doi.org/10.5194/acp-15-1573-2015, 2015.

Cui, Y. Y., Liu, S., Bai, Z., Bian, J., Li, D., Fan, K., McKeen, S. A., Watts, L. A., Ciciora, S. J., and Gao, R.-S.: Religious burning as a potential major source of atmospheric fine aerosols in summertime Lhasa on the Tibetan Plateau, Atmos. Environ., 181, 186-191, https://doi.org/10.1016/j.atmosenv.2018.03.025, 2018.

Dal Maso, M., Kulmala, M., Riipinen, I., Wagner, R., Hussein, T., Aalto, P. P., and Lehtinen, K. E. J.: Formation and growth of fresh atmospheric aerosols: eight years of aerosol size distribution data from SMEAR II, Hyytiala, Finland, Boreal Environ. Res., 10, 323-336, 2005.

Deng, Z. Z., Zhao, C. S., Ma, N., Liu, P. F., Ran, L., Xu, W. Y., Chen, J., Liang, Z., Liang, S., Huang, M. Y., Ma, X. C., Zhang, Q., Quan, J. N., Yan, P., Henning, S., Mildenberger, K., Sommerhage, E., Schäfer, M., Stratmann, F., and Wiedensohler, A.: Size-resolved and bulk activation properties of aerosols in the North China Plain, Atmos. Chem. Phys., 11, 3835-3846, https://doi.org/10.5194/acp-11-3835-2011, 2011.

Draxler, R. R., and Rolph, G. D.: HYSPLIT (HYbrid Single-Particle Lagrangian Integrated Trajectory) model access via NOAA ARL READY website (http://www.arl.noaa.gov/ready/hysplit4.html). in, NOAA Air Resources Laboratory, Silver Spring, MD, USA, 2003.

Du, W., Sun, Y. L., Xu, Y. S., Jiang, Q., Wang, Q. Q., Yang, W., Wang, F., Bai, Z. P., Zhao, X. D., and Yang, Y. C.: Chemical characterization of submicron aerosol and particle growth events at a national background site (3295 m a.s.l.) on the Tibetan Plateau, Atmos. Chem. Phys., 15, 10811-10824, https://doi.org/10.5194/acp-15-10811-2015, 2015.

Duan, A. M., and Wu, G. X.: Role of the Tibetan Plateau thermal forcing in the summer climate patterns over subtropical Asia, Clim. Dyn., 24, 793-807, https://doi.org/10.1007/s00382-004-0488-8, 2005.

Freney, E. J., Sellegri, K., Canonaco, F., Boulon, J., Hervo, M., Weigel, R., Pichon, J. M., Colomb, A., Prévôt, A. S. H., and Laj, P.: Seasonal variations in aerosol particle composition at the puy-de-Dôme research station in France, Atmos. Chem. Phys., 11, 13047-13059, https://doi.org/10.5194/acp-11-13047-2011, 2011.

Fröhlich, R., Cubison, M. J., Slowik, J. G., Bukowiecki, N., Canonaco, F., Croteau, P. L., Gysel, M., Henne, S., Herrmann, E., Jayne, J. T., Steinbacher, M., Worsnop, D. R., Baltensperger, U., and Prévôt, A. S. H.: Fourteen months of on-line measurements of the non-refractory submicron aerosol at the Jungfraujoch (3580 m a.s.l.) – chemical composition, origins and organic aerosol sources, Atmos. Chem. Phys., 15, 11373-11398, https://doi.org/10.5194/acp-15-11373-2015, 2015.

Gunthe, S. S., Rose, D., Su, H., Garland, R. M., Achtert, P., Nowak, A., Wiedensohler, A., Kuwata, M., Takegawa, N., Kondo, Y., Hu, M., Shao, M., Zhu, T., Andreae, M. O., and Pöschl, U.: Cloud condensation nuclei (CCN) from fresh and aged air pollution in the megacity region of Beijing, Atmos. Chem. Phys., 11, 11023-11039, https://doi.org/10.5194/acp-11-11023-2011, 2011.

He, L. Y., Lin, Y., Huang, X. F., Guo, S., Xue, L., Su, Q., Hu, M., Luan, S. J., and Zhang, Y. H.: Characterization of high-resolution aerosol mass spectra of primary organic aerosol emissions from Chinese cooking and biomass burning, Atmos. Chem. Phys., 10, 11535-11543, https://doi.org/10.5194/acp-10-11535-2010, 2010.

Jimenez, J. L., Canagaratna, M. R., Donahue, N. M., Prevot, A. S., Zhang, Q., Kroll, J. H., DeCarlo, P. F., Allan, J. D., Coe, H., Ng, N. L., Aiken, A. C., Docherty, K. S., Ulbrich, I. M., Grieshop, A. P., Robinson, A. L., Duplissy, J., Smith, J. D., Wilson, K. R., Lanz, V. A., Hueglin, C., Sun, Y. L., Tian, J., Laaksonen, A., Raatikainen, T., Rautiainen, J., Vaattovaara, P., Ehn, M., Kulmala, M., Tomlinson, J. M., Collins, D. R., Cubison, M. J., Dunlea, E. J., Huffman, J. A., Onasch, T. B., Alfarra, M. R., Williams, P. I., Bower, K., Kondo, Y., Schneider, J., Drewnick, F., Borrmann, S., Weimer, S., Demerjian, K., Salcedo, D., Cottrell, L., Griffin, R., Takami, A., Miyoshi, T., Hatakeyama, S., Shimono, A., Sun, J. Y., Zhang, Y. M., Dzepina, K., Kimmel, J. R., Sueper, D., Jayne, J. T., Herndon, S. C., Trimborn, A. M., Williams, L. R., Wood, E. C., Middlebrook, A. M., Kolb, C. E., Baltensperger, U., and Worsnop, D. R.: Evolution of organic aerosols in the atmosphere, Science, 326, 1525-1529, https://doi.org/10.1126/science.1180353, 2009.

Jimenez, J. L., Canagaratna, M. R., Drewnick, F., Allan, J. D., Alfarra, M. R., Middlebrook, A. M., Slowik, J. G., Zhang, Q., Coe, H., Jayne, J. T., and Worsnop, D. R.: Comment on "The Effects of Molecular Weight and Thermal Decomposition on the Sensitivity of a Thermal Desorption Aerosol Mass Spectrometer". Aerosol Sci. Technol., 50(9), i–xv, http://doi:10.1080/02786826.2016.1205728, 2016.

Kang, S., Xu, Y., You, Q., Flügel, W.-A., Pepin, N., and Yao, T.: Review of climate and cryospheric

change in the Tibetan Plateau, Environ. Res. Lett., 5, 015101, https://doi.org/10.1088/1748-9326/5/1/015101, 2010.

Kang, S., Chen, P., Li, C., Liu, B., and Cong, Z.: Atmospheric Aerosol Elements over the Inland Tibetan Plateau: Concentration, Seasonality, and Transport, Aerosol Air Qual. Res., 16, 789-800, https://doi.org/10.4209/aaqr.2015.05.0307, 2016.

Kang, S., Cong, Z., Wang, X., Zhang, Q., Ji, Z., Zhang, Y., and Xu, B.: The transboundary transport of air pollutants and their environmental impacts on Tibetan Plateau, Chin. Sci. Bull., 64, 2876-2884, https://doi.org/10.1360/tb-2019-0135, 2019a.

Kang, S., Zhang, Q., Qian, Y., Ji, Z., Li, C., Cong, Z., Zhang, Y., Guo, J., Du, W., Huang, J., You, Q., Panday, A. K., Rupakheti, M., Chen, D., Gustafsson, Ö., Thiemens, M. H., and Qin, D.: Linking atmospheric pollution to cryospheric change in the Third Pole region: current progress and future prospects, Natl. Sci. Rev., 6, 796-809, https://doi.org/10.1093/nsr/nwz031, 2019b.

Kang, S., Zhang, Y., Chen, P., Guo, J., Zhang, Q., Cong, Z., Kaspari, S., Tripathee, L., Gao, T., Niu, H., Zhong, X., Chen, X., Hu, Z., Li, X., Li, Y., Neupane, B., Yan, F., Rupakheti, D., Gul, C., Zhang, W., Wu, G., Yang, L., Wang, Z., and Li, C.: Black carbon and organic carbon dataset over the Third Pole, Earth System Science Data, 14, 683-707, https://doi.org/10.5194/essd-14-683-2022, 2022.

Kopacz, M., Mauzerall, D. L., Wang, J., Leibensperger, E. M., Henze, D. K., and Singh, K.: Origin and radiative forcing of black carbon transported to the Himalayas and Tibetan Plateau, Atmos. Chem. Phys., 11, 2837-2852, https://doi.org/10.5194/acp-11-2837-2011, 2011.

Lau, K. M., Kim, M. K., and Kim, K. M.: Asian summer monsoon anomalies induced by aerosol direct forcing: the role of the Tibetan Plateau, Clim. Dyn., 26, 855-864, https://doi.org/10.1007/s00382-006-0114-z, 2006.

Li, C., Bosch, C., Kang, S., Andersson, A., Chen, P., Zhang, Q., Cong, Z., Chen, B., Qin, D., and Gustafsson, O.: Sources of black carbon to the Himalayan-Tibetan Plateau glaciers, Nat. Commun., 7, 12574, https://doi.org/10.1038/ncomms12574, 2016a.

Li, C., Yan, F., Kang, S., Chen, P., Hu, Z., Gao, S., Qu, B., and Sillanpää, M.: Light absorption characteristics of carbonaceous aerosols in two remote stations of the southern fringe of the Tibetan Plateau, China, Atmos. Environ., 143, 79-85, https://doi.org/10.1016/j.atmosenv.2016.08.042, 2016b.

Li, X., Kang, S., Zhang, G., Qu, B., Tripathee, L., Paudyal, R., Jing, Z., Zhang, Y., Yan, F., Li, G., Cui, X., Xu, R., Hu, Z., and Li, C.: Light-absorbing impurities in a southern Tibetan Plateau glacier: Variations and potential impact on snow albedo and radiative forcing, Atmos. Res., 200, 77-87, https://doi.org/10.1016/j.atmosres.2017.10.002, 2018.

Li, Y. J., Sun, Y., Zhang, Q., Li, X., Li, M., Zhou, Z., and Chan, C. K.: Real-time chemical characterization of atmospheric particulate matter in China: A review, Atmos. Environ., 158, 270-304, https://doi.org/10.1016/j.atmosenv.2017.02.027, 2017.

Liu, Y., Sato, Y., Jia, R., Xie, Y., Huang, J., and Nakajima, T.: Modeling study on the transport of summer dust and anthropogenic aerosols over the Tibetan Plateau, Atmos. Chem. Phys., 15, 12581-12594, https://doi.org/10.5194/acp-15-12581-2015, 2015.

Liu, Y., Hua, S., Jia, R., and Huang, J.: Effect of Aerosols on the Ice Cloud Properties Over the Tibetan Plateau, J. Geophys. Res. Atmos., 124, 9594-9608, https://doi.org/10.1029/2019jd030463, 2019.

Middlebrook, A. M., Bahreini, R., Jimenez, J. L., and Canagaratna, M. R.: Evaluation of Composition-Dependent Collection Efficiencies for the Aerodyne Aerosol Mass Spectrometer using Field Data, Aerosol Sci. Technol., 46, 258-271, https://doi.org/10.1080/02786826.2011.620041, 2012.

Pöhlker, M. L., Pöhlker, C., Ditas, F., Klimach, T., Hrabe de Angelis, I., Araújo, A., Brito, J., Carbone, S., Cheng, Y., Chi, X., Ditz, R., Gunthe, S. S., Kesselmeier, J., Könemann, T., Lavrič, J. V., Martin, S. T., Mikhailov, E., Moran-Zuloaga, D., Rose, D., Saturno, J., Su, H., Thalman, R., Walter, D., Wang, J., Wolff, S., Barbosa, H. M. J., Artaxo, P., Andreae, M. O., and Pöschl, U.: Long-term observations of cloud condensation nuclei in the Amazon rain forest – Part 1: Aerosol size distribution, hygroscopicity, and new model parametrizations for CCN prediction, Atmos. Chem. Phys., 16, 15709-15740, https://doi.org/10.5194/acp-16-15709-2016, 2016.

Qiu, J.: The third pole, Nature, 454, 393-396, https://doi.org/10.1038/454393a, 2008.

Ramanathan, V., Ramana, M. V., Roberts, G., Kim, D., Corrigan, C., Chung, C., and Winker, D.: Warming trends in Asia amplified by brown cloud solar absorption, Nature, 448, 575-578, https://doi.org/10.1038/nature06019, 2007.

Ricchiazzi, P., Yang, S., Gautier, C., and Sowle, D.: SBDART: A Research and Teaching Software Tool for Plane-Parallel Radiative Transfer in the Earth's Atmosphere, Bull. Am. Meteorol. Soc., 79, 2101-2114, https://doi.org/10.1175/1520-0477(1998)079<2101:Sarats>2.0.Co;2, 1998.

Rinaldi, M., Gilardoni, S., Paglione, M., Sandrini, S., Fuzzi, S., Massoli, P., Bonasoni, P., Cristofanelli, P., Marinoni, A., Poluzzi, V., and Decesari, S.: Organic aerosol evolution and transport observed at Mt. Cimone (2165 m a.s.l.), Italy, during the PEGASOS campaign, Atmos. Chem. Phys., 15, 11327-11340,

https://doi.org/10.5194/acp-15-11327-2015, 2015.

Rose, D., Gunthe, S. S., Mikhailov, E., Frank, G. P., Dusek, U., Andreae, M. O., and Pöschl, U.: Calibration and measurement uncertainties of a continuous-flow cloud condensation nuclei counter (DMT-CCNC): CCN activation of ammonium sulfate and sodium chloride aerosol particles in theory and experiment, Atmos. Chem. Phys., 8, 1153–1179, https://doi.org/10.5194/acp-8-1153-2008, 2008.

Rose, D., Nowak, A., Achtert, P., Wiedensohler, A., Hu, M., Shao, M., Zhang, Y., Andreae, M. O., and Poschl, U.: Cloud condensation nuclei in polluted air and biomass burning smoke near the mega-city Guangzhou, China - Part 1: Size-resolved measurements and implications for the modeling of aerosol particle hygroscopicity and CCN activity, Atmos. Chem. Phys., 10, 3365-3383, https://doi.org/10.5194/acp-10-3365-2010, 2010.

Schmale, J., Schneider, J., Nemitz, E., Tang, Y. S., Dragosits, U., Blackall, T. D., Trathan, P. N., Phillips, G. J., Sutton, M., and Braban, C. F.: Sub-Antarctic marine aerosol: dominant contributions from biogenic sources, Atmos. Chem. Phys., 13, 8669-8694, https://doi.org/10.5194/acp-13-8669-2013, 2013.

Schueneman, M. K., Nault, B. A., Campuzano-Jost, P., Jo, D. S., Day, D. A., Schroder, J. C., Palm, B. B., Hodzic, A., Dibb, J. E., and Jimenez, J. L.: Aerosol pH indicator and organosulfate detectability from aerosol mass spectrometry measurements, Atmos. Meas. Tech., 14, 2237-2260, https://doi.org/10.5194/amt-14-2237-2021, 2021.

Selimovic, V., Yokelson, R. J., Warneke, C., Roberts, J. M., de Gouw, J., Reardon, J., and Griffith, D. W. T.: Aerosol optical properties and trace gas emissions by PAX and OP-FTIR for laboratory-simulated western US wildfires during FIREX, Atmos. Chem. Phys., 18, 2929–2948, https://doi.org/10.5194/acp-18-2929-2018, 2018.

Sun, Y. L., Zhang, Q., Macdonald, A. M., Hayden, K., Li, S. M., Liggio, J., Liu, P. S. K., Anlauf, K. G., Leaitch, W. R., Steffen, A., Cubison, M., Worsnop, D. R., van Donkelaar, A., and Martin, R. V.: Size-resolved aerosol chemistry on Whistler Mountain, Canada with a high-resolution aerosol mass spectrometer during INTEX-B, Atmos. Chem. Phys., 9, 3095-3111, https://doi.org/10.5194/acp-9-3095-2009, 2009.

Sun, Y. L., Zhang, Q., Schwab, J. J., Demerjian, K. L., Chen, W. N., Bae, M. S., Hung, H. M., Hogrefe, O., Frank, B., Rattigan, O. V., and Lin, Y. C.: Characterization of the sources and processes of organic and inorganic aerosols in New York city with a high-resolution time-of-flight aerosol mass apectrometer, Atmos. Chem. Phys., 11, 1581-1602, https://doi.org/10.5194/acp-11-1581-2011, 2011.

Takami, A., Miyoshi, T., Shimono, A., and Hatakeyama, S.: Chemical composition of fine aerosol measured by AMS at Fukue Island, Japan during APEX period, Atmos. Environ., 39, 4913-4924, https://doi.org/10.1016/j.atmosenv.2005.04.038, 2005.

Van Damme, M., Erisman, J. W., Clarisse, L., Dammers, E., Whitburn, S., Clerbaux, C., Dolman, A. J., and Coheur, P.-F.: Worldwide spatiotemporal atmospheric ammonia (NH_3) columns variability revealed by satellite, Geophys. Res. Lett., 42, 8660-8668, https://doi.org/10.1002/2015gl065496, 2015.

Wan, X., Kang, S., Wang, Y., Xin, J., Liu, B., Guo, Y., Wen, T., Zhang, G., and Cong, Z.: Size distribution of carbonaceous aerosols at a high-altitude site on the central Tibetan Plateau (Nam Co Station, 4730ma.s.l.), Atmos. Res., 153, 155-164, https://doi.org/10.1016/j.atmosres.2014.08.008, 2015.

Wang, J., Ge, X., Chen, Y., Shen, Y., Zhang, Q., Sun, Y., Xu, J., Ge, S., Yu, H., and Chen, M.: Highly time-resolved urban aerosol characteristics during springtime in Yangtze River Delta, China: insights from soot particle aerosol mass spectrometry, Atmos. Chem. Phys., 16, 9109-9127, https://doi.org/10.5194/acp-16-9109-2016, 2016.

Wang, J., Zhang, Q., Chen, M., Collier, S., Zhou, S., Ge, X., Xu, J., Shi, J., Xie, C., Hu, J., Ge, S., Sun, Y., and Coe, H.: First Chemical Characterization of Refractory Black Carbon Aerosols and Associated Coatings over the Tibetan Plateau (4730 m a.s.l), Environ. Sci. Technol., 51, 14072-14082, https://doi.org/10.1021/acs.est.7b03973, 2017.

Xie, C., Xu, W., Wang, J., Wang, Q., Liu, D., Tang, G., Chen, P., Du, W., Zhao, J., Zhang, Y., Zhou, W., Han, T., Bian, Q., Li, J., Fu, P., Wang, Z., Ge, X., Allan, J., Coe, H., and Sun, Y.: Vertical characterization of aerosol optical properties and brown carbon in winter in urban Beijing, China, Atmos. Chem. Phys., 19, 165-179, https://doi.org/10.5194/acp-19-165-2019, 2019.

Xu, B., Cao, J., Hansen, J., Yao, T., Joswia, D. R., Wang, N., Wu, G., Wang, M., Zhao, H., Yang, W., Liu, X., and He, J.: Black soot and the survival of Tibetan glaciers, Proc. Natl. Acad. Sci. USA, 106, 22114-22118, https://doi.org/10.1073/pnas.0910444106, 2009.

Xu, J., Wang, Z., Yu, G., Qin, X., Ren, J., and Qin, D.: Characteristics of water soluble ionic species in fine particles from a high altitude site on the northern boundary of Tibetan Plateau: Mixture of mineral dust and anthropogenic aerosol, Atmos. Res., 143, 43-56, https://doi.org/10.1016/j.atmosres.2014.01.018, 2014a.

Xu, J., Zhang, Q., Chen, M., Ge, X., Ren, J., and Qin, D.: Chemical composition, sources, and processes

of urban aerosols during summertime in northwest China: insights from high-resolution aerosol mass spectrometry, Atmos. Chem. Phys., 14, 12593-12611, https://doi.org/10.5194/acp-14-12593-2014, 2014b.

Xu, J., Zhang, Q., Wang, Z. B., Yu, G. M., Ge, X. L., and Qin, X.: Chemical composition and size distribution of summertime $PM_{2.5}$ at a high altitude remote location in the northeast of the Qinghai-Xizang (Tibet) Plateau: insights into aerosol sources and processing in free troposphere, Atmos. Chem. Phys., 15, 5069-5081, https://doi.org/10.5194/acp-15-5069-2015, 2015.

Xu, J., Shi, J., Zhang, Q., Ge, X., Canonaco, F., Prévôt, A. S. H., Vonwiller, M., Szidat, S., Ge, J., Ma, J., An, Y., Kang, S., and Qin, D.: Wintertime organic and inorganic aerosols in Lanzhou, China: sources, processes, and comparison with the results during summer, Atmos. Chem. Phys., 16, 14937-14957, https://doi.org/10.5194/acp-16-14937-2016, 2016.

Xu, J., Zhang, Q., Shi, J., Ge, X., Xie, C., Wang, J., Kang, S., Zhang, R., and Wang, Y.: Chemical characteristics of submicron particles at the central Tibetan Plateau: insights from aerosol mass spectrometry, Atmos. Chem. Phys., 18, 427-443, https://doi.org/10.5194/acp-18-427-2018, 2018.

Xu, J., Hettiyadura, A. P. S., Liu, Y., Zhang, X., Kang, S., and Laskin, A.: Regional Differences of Chemical Composition and Optical Properties of Aerosols in the Tibetan Plateau, J. Geophys. Res. Atmos., 125, https://doi.org/10.1029/2019jd031226, 2020.

Xu, J.: High-time-resolution dataset of atmospheric aerosols over the Tibetan Plateau and its surroundings (2015-2021), National Cryosphere Desert Data Center [Data set], https://doi.org/10.12072/ncdc.NIEER.db2200.2022, 2022.

Xu, J., Hettiyadura, A. P. S., Liu, Y., Zhang, X., Kang, S., and Laskin, A.: Atmospheric Brown Carbon on the Tibetan Plateau: Regional Differences in Chemical Composition and Light Absorption Properties, Environmental Science & Technology Letters, 9, 219-225, https://doi.org/10.1021/acs.estlett.2c00016, 2022.

Yao, T., Thompson, L., Mosbrugger, V., Zhang, F., Ma, Y., Luo, T., Xu, B., Yang, X., Joswiak, D. R., Wang, W., Joswiak, M. E., Devkota, L. P., Tayal, S., Jilani, R., and Fayziev, R.: Third Pole Environment (TPE), Environ. Dev., 3, 52-64, https://doi.org/10.1016/j.envdev.2012.04.002, 2012.

Yao, T., Xue, Y., Chen, D., Chen, F., Thompson, L., Cui, P., Koike, T., Lau, W. K. M., Lettenmaier, D., Mosbrugger, V., Zhang, R., Xu, B., Dozier, J., Gillespie, T., Gu, Y., Kang, S., Piao, S., Sugimoto, S., Ueno, K., Wang, L., Wang, W., Zhang, F., Sheng, Y., Guo, W., Ailikun, Yang, X., Ma, Y., Shen, S. S. P., Su, Z., Chen, F., Liang, S., Liu, Y., Singh, V. P., Yang, K., Yang, D., Zhao, X., Qian, Y., Zhang, Y., and Li, Q.: Recent Third Pole's Rapid Warming Accompanies Cryospheric Melt and Water Cycle Intensification and Interactions between Monsoon and Environment: Multidisciplinary Approach with Observations, Modeling, and Analysis, Bull. Am. Meteorol. Soc., 100, 423-444, https://doi.org/10.1175/bams-d-17-0057.1, 2019.

You, Q., Cai, Z., Pepin, N., Chen, D., Ahrens, B., Jiang, Z., Wu, F., Kang, S., Zhang, R., Wu, T., Wang, P., Li, M., Zuo, Z., Gao, Y., Zhai, P., and Zhang, Y.: Warming amplification over the Arctic Pole and Third Pole: Trends, mechanisms and consequences, Earth-Science Reviews, 217, 103625, https://doi.org/10.1016/j.earscirev.2021.103625, 2021.

Zhang, N., Cao, J., Liu, S., Zhao, Z., Xu, H., and Xiao, S.: Chemical composition and sources of $PM_{2.5}$ and TSP collected at Qinghai Lake during summertime, Atmos. Res., 138, 213-222, https://doi.org/10.1016/j.atmosres.2013.11.016, 2014.

Zhang, Q., Alfarra, M. R., Worsnop, D. R., Allan, J. D., Coe, H., Canagaratna, M. R., and Jimenez, J. L.: Deconvolution and quantification of hydrocarbon-like and oxygenated organic aerosols based on aerosol mass spectrometry, Environ. Sci. Technol., 39, 4938-4952, https://doi.org/10.1021/es048568l, 2005a.

Zhang, Q., Canagaratna, M. R., Jayne, J. T., Worsnop, D. R., and Jimenez, J. L.: Time- and size-resolved chemical composition of submicron particles in Pittsburgh: Implications for aerosol sources and processes, J. Geophys. Res. Atmos., 110, D07S09, https://doi.org/10.1029/2004jd004649, 2005b.

Zhang, Q., Jimenez, J. L., Canagaratna, M. R., Allan, J. D., Coe, H., Ulbrich, I., Alfarra, M. R., Takami, A., Middlebrook, A. M., Sun, Y. L., Dzepina, K., Dunlea, E., Docherty, K., DeCarlo, P. F., Salcedo, D., Onasch, T., Jayne, J. T., Miyoshi, T., Shimono, A., Hatakeyama, S., Takegawa, N., Kondo, Y., Schneider, J., Drewnick, F., Borrmann, S., Weimer, S., Demerjian, K., Williams, P., Bower, K., Bahreini, R., Cottrell, L., Griffin, R. J., Rautiainen, J., Sun, J. Y., Zhang, Y. M., and Worsnop, D. R.: Ubiquity and dominance of oxygenated species in organic aerosols in anthropogenically-influenced Northern Hemisphere midlatitudes, Geophys. Res. Lett., 34, L13801, https://doi.org/10.1029/2007gl029979, 2007a.

Zhang, Q., Jimenez, J. L., Worsnop, D., and Canagaratna, M.: A case study of urban particle acidity and its influence on secondary organic aerosol, Environ. Sci. Technol., 41, 3213-3219, https://doi.org/10.1021/es061812j, 2007b.

1384 Zhang, X., Xu, J., Kang, S., Liu, Y., and Zhang, Q.: Chemical characterization of long-range transport
1385   biomass burning emissions to the Himalayas: insights from high-resolution aerosol mass spectrometry,
1386   Atmos. Chem. Phys., 18, 4617–4638, https://doi.org/10.5194/acp-18-4617-2018, 2018.
1387 Zhang, X., Xu, J., Kang, S., Zhang, Q., and Sun, J.: Chemical characterization and sources of submicron
1388   aerosols in the northeastern Qinghai–Tibet Plateau: insights from high-resolution mass spectrometry,
1389   Atmos. Chem. Phys., 19, 7897-7911, https://doi.org/10.5194/acp-19-7897-2019, 2019.
1390 Zhang, X., Xu, J., and Kang, S.: Chemical characterization of submicron particulate matter (PM_1) emitted
1391   by burning highland barley in the northeastern part of the Qinghai–Tibet Plateau, Atmos. Environ.,
1392   224, 117351, https://doi.org/10.1016/j.atmosenv.2020.117351, 2020.
1393 Zhang, X., Xu, J., Kang, S., Sun, J., Shi, J., Gong, C., Sun, X., Du, H., Ge, X., and Zhang, Q.: Regional
1394   Differences in the Light Absorption Properties of Fine Particulate Matter Over the Tibetan Plateau:
1395   Insights From HR-ToF-AMS and Aethalometer Measurements, J. Geophys. Res. Atmos., 126,
1396   https://doi.org/10.1029/2021jd035562, 2021.
1397 Zhao, W., Zhang, X., Zhai, L., Shen, X., and Xu, J.: Chemical characterization and sources of submicron
1398   aerosols in Lhasa on the Qinghai–Tibet Plateau: Insights from high-resolution mass spectrometry, Sci.
1399   Total Environ., 815, https://doi.org/10.1016/j.scitotenv.2021.152866, 2022.
1400 Zhao, Z., Cao, J., Shen, Z., Xu, B., Zhu, C., Chen, L.-W. A., Su, X., Liu, S., Han, Y., Wang, G., and Ho,
1401   K.: Aerosol particles at a high-altitude site on the Southeast Tibetan Plateau, China: Implications for
1402   pollution transport from South Asia, J. Geophys. Res. Atmos., 118, 11360-11375,
1403   https://doi.org/10.1002/jgrd.50599, 2013.
1404 Zheng, J., Hu, M., Du, Z., Shang, D., Gong, Z., Qin, Y., Fang, J., Gu, F., Li, M., Peng, J., Li, J., Zhang,
1405   Y., Huang, X., He, L., Wu, Y., and Guo, S.: Influence of biomass burning from South Asia at a high-
1406   altitude mountain receptor site in China, Atmos. Chem. Phys., 17, 6853-6864,
1407   https://doi.org/10.5194/acp-17-6853-2017, 2017.
1408 Zhou, S., Collier, S., Jaffe, D. A., Briggs, N. L., Hee, J., Sedlacek Iii, A. J., Kleinman, L., Onasch, T. B.,
1409   and Zhang, Q.: Regional influence of wildfires on aerosol chemistry in the western US and insights
1410   into atmospheric aging of biomass burning organic aerosol, Atmos. Chem. Phys., 17, 2477-2493,
1411   https://doi.org/10.5194/acp-17-2477-2017, 2017.
1412 Zhou, T., and Zhang, W.: Anthropogenic warming of Tibetan Plateau and constrained future projection,
1413   Environ. Res. Lett., 16, 044039, https://doi.org/10.1088/1748-9326/abede8, 2021.
1414 Zhou, W., Xu, W., Kim, H., Zhang, Q., Fu, P., Worsnop, D. R., and Sun, Y.: A review of aerosol chemistry
1415   in Asia: insights from aerosol mass spectrometer measurements, Environ. Sci.: Proc. Imp.,
1416   https://doi.org/10.1039/D0EM00212G, 2020.
1417 Zhu, C.-S., Cao, J.-J., Ho, K.-F., Antony Chen, L. W., Huang, R.-J., Wang, Y.-C., Li, H., Shen, Z.-X.,
1418   Chow, J. C., Watson, J. G., Su, X.-l., Wang, Q.-y., and Xiao, S.: The optical properties of urban aerosol
1419   in northern China: A case study at Xi'an, Atmos. Res., 160, 59-67,
1420   https://doi.org/10.1016/j.atmosres.2015.03.008, 2015.
1421 Zhu, Q., He, L. Y., Huang, X. F., Cao, L. M., Gong, Z. H., Wang, C., Zhuang, X., and Hu, M.:
1422   Atmospheric aerosol compositions and sources at two national background sites in northern and
1423   southern China, Atmos. Chem. Phys., 16, 10283-10297, https://doi.org/10.5194/acp-16-10283-2016,
1424   2016.
1425
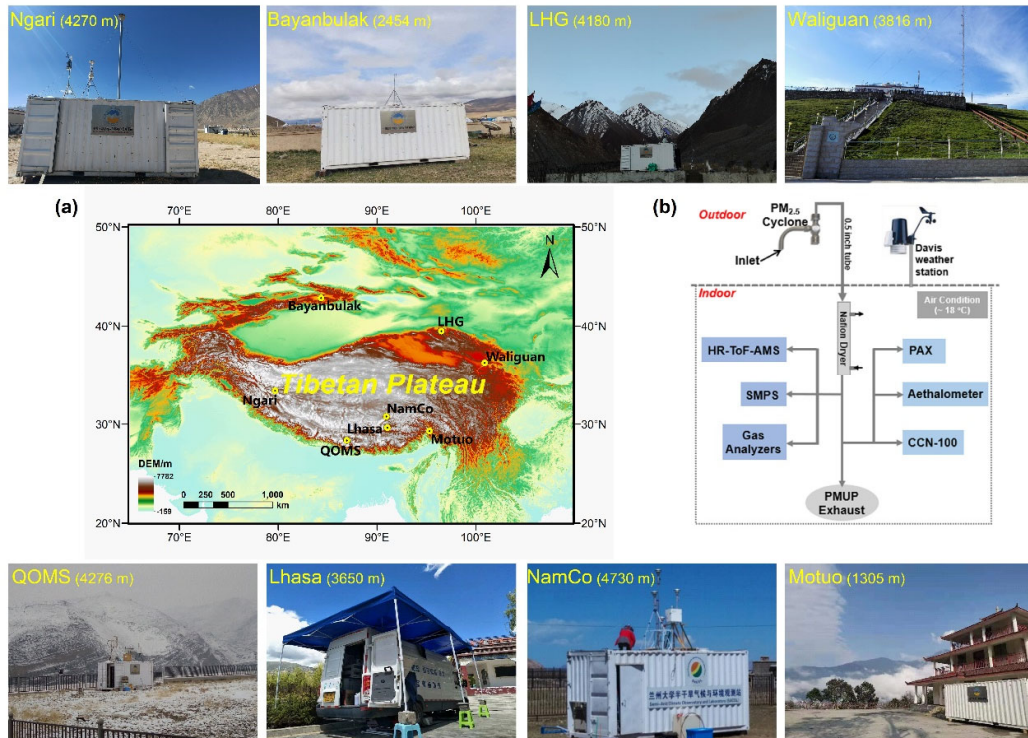
Figures

1427

Figure 1. (a) Geographical locations of the observation sites (see Table 1 for full name and characteristics of each site) in the Tibetan Plateau and its surroundings in this study (The geographical base map is created with ArcGIS). Fieldwork photographs illustrate the real observation conditions and surroundings at each site. **(b)** The normal sampling setups of instruments during the online aerosol observations.
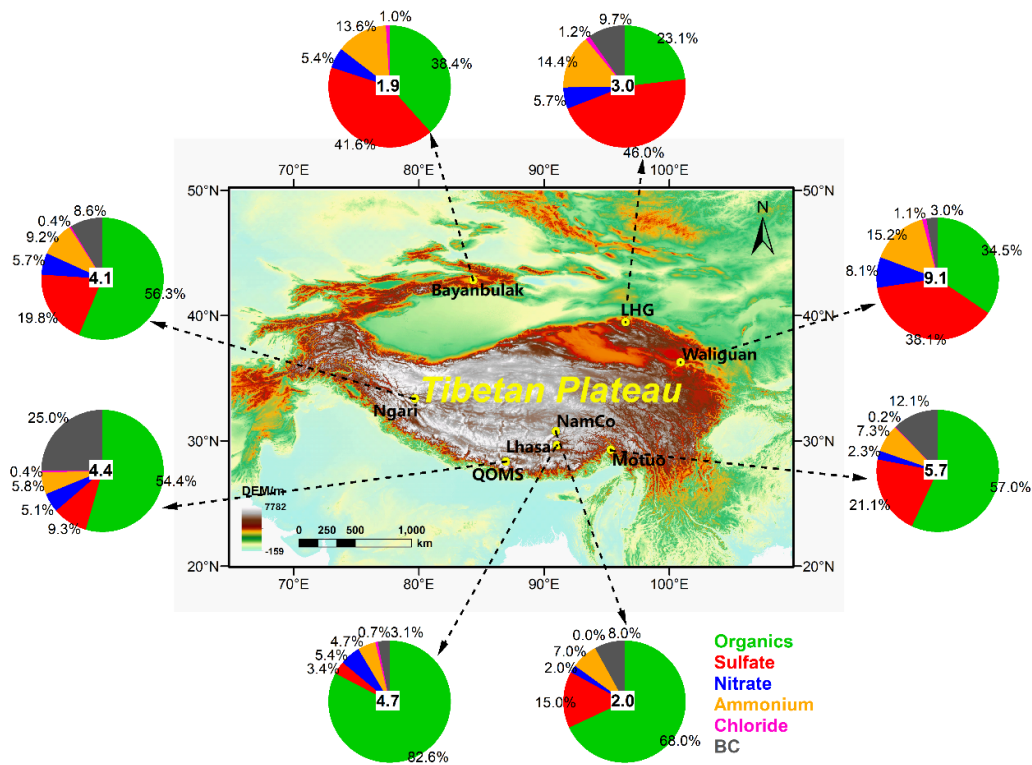
1433

1434 **Figure 2.** Regional distribution of average mass concentrations (values marked in the central of

1435 each pie chart with unit of µg m⁻³) and chemical compositions (percentage values around each pie

1436 chart) of submicron aerosols (PM₁) during the eight online aerosol field measurements in the Tibetan

1437 Plateau and its surroundings (The geographical base map is created with ArcGIS). The concentration

1438 at each site is presented in ambient condition.
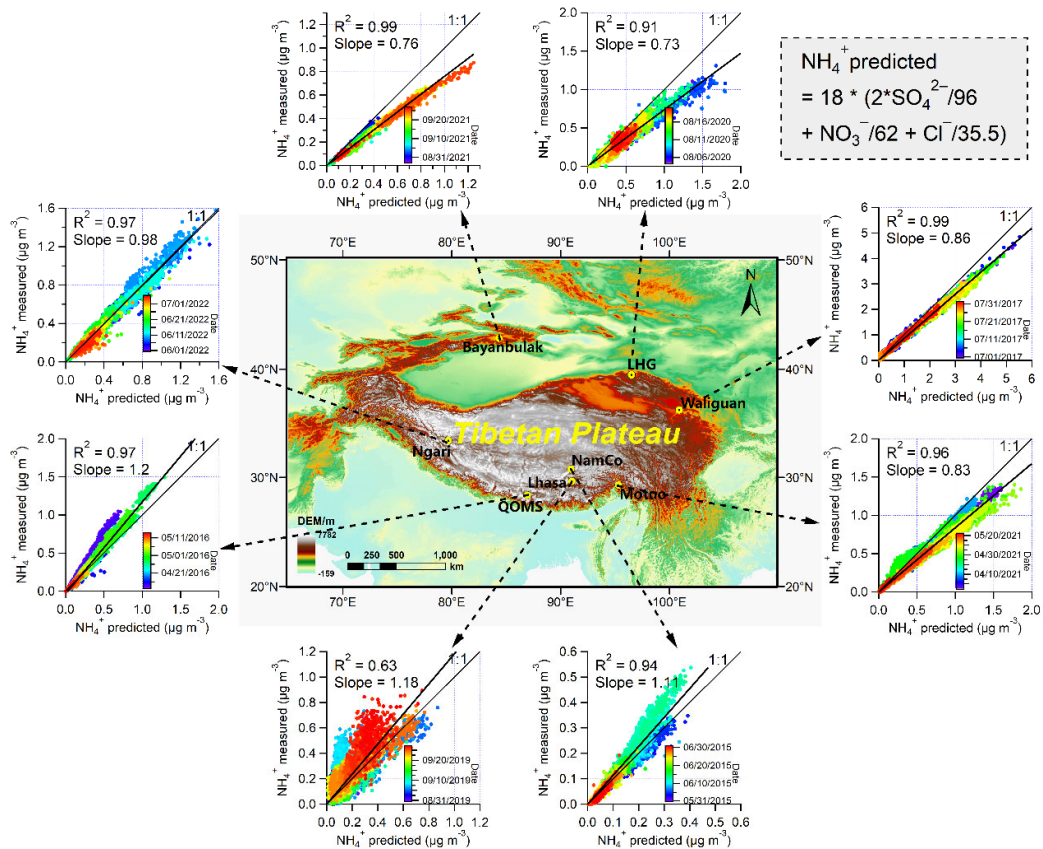
1439

Figure 3. Regional difference of bulk acidity of submicron aerosols based on the scatterplot analysis and linear regression of measured NH_4^+ versus predicted NH_4^+ during the eight aerosol field measurement campaigns in the Tibetan Plateau and its surroundings (The geographical base map is created with ArcGIS).
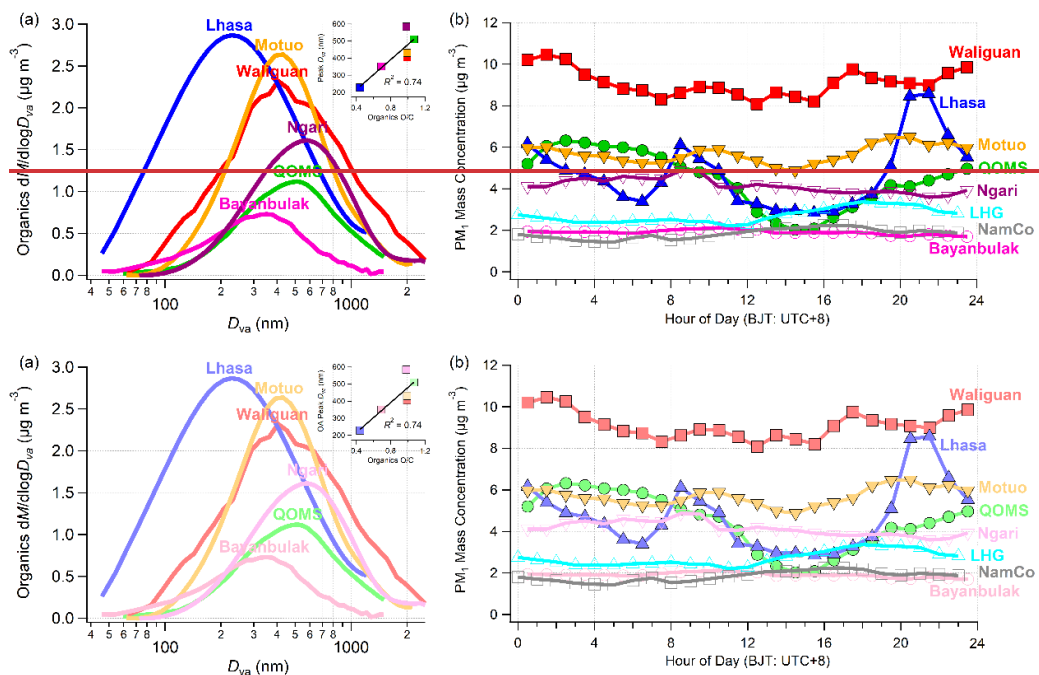
1444

1445

Figure 4. (a) Average size distributions of organic mass concentrations during six field measurement campaigns in the Tibetan Plateau and its surroundings. (b) Diurnal variations of total PM$_1$ mass concentrations during the eight field measurement campaigns in the Tibetan Plateau and its surroundings. Insert graph in (a) is the scatter plot of peak diameters in ~~these~~their size distributions versus the average O/C ratio of organics.
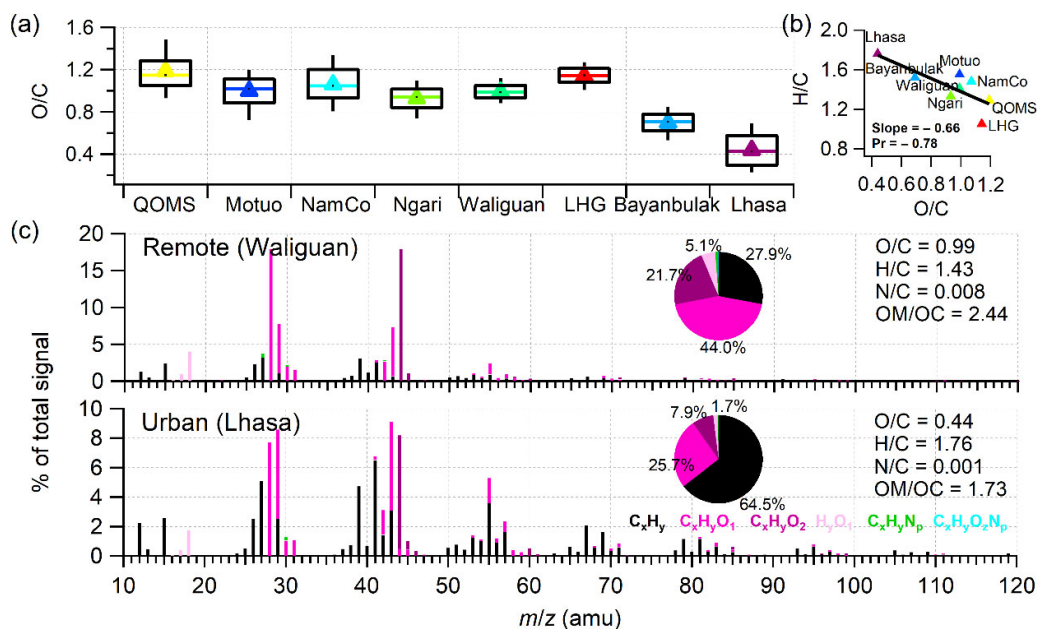
1451

Figure 5. (a) Box plots of the average O/C ratios and (b) Van Krevelen diagram of H/C versus O/C among the eight field measurement campaigns in this study. (c) The average HRMSs of OA colored

1454   with different ion categories during the Waliguan and Lhasa measurement campaigns. The whiskers

1455   of boxes indicate the 90th and 10th percentiles, the upper and lower boundaries of boxes indicate the

1456   75th and 25th percentiles, the lines in the boxes indicate the median values, the markers indicate the

1457   mean values, and similarly hereinafter.
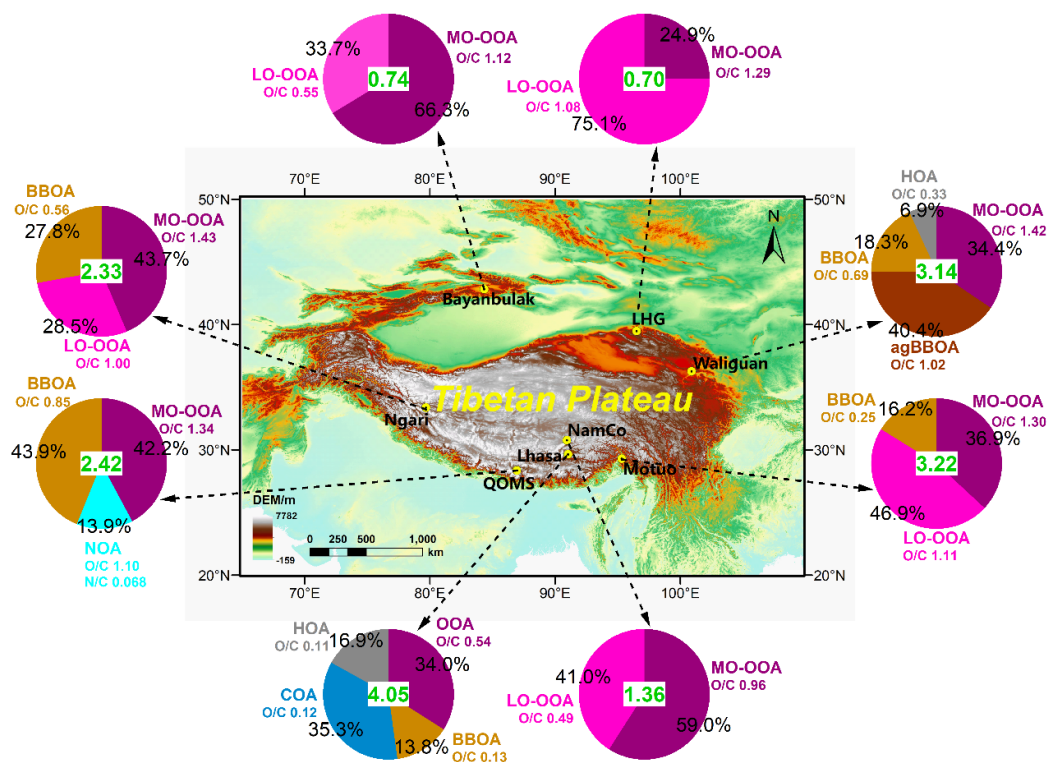
1458

Figure 6. Regional distribution of OA components from PMF source apportionment during the eight online aerosol field measurements in the Tibetan Plateau and its surroundings (The geographical base map is created with ArcGIS). Values marked in the central of each pie chart are average OA mass with unit of $\mu g\ m^{-3}$, while the percentage values around the pie chart are the mass contributions of each OA component. The O/C ratio of each OA component is also marked around each pie chart.
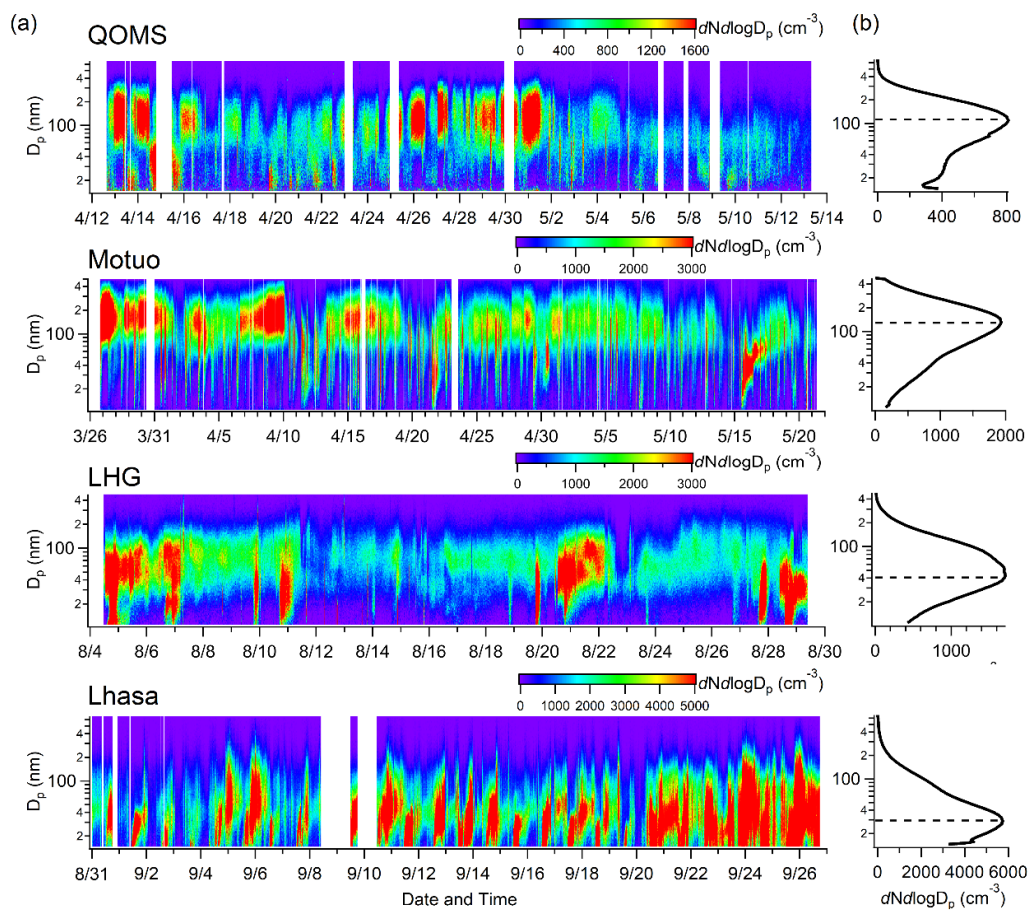
1464

1465 **Figure 7. (a)** Temporal variations of the size distributions of particle number concentrations during

1466 the aerosol field measurement campaigns at QOMS, Motuo, LHG, and Lhasa sites. **(b)** The average

1467 size distribution of particle number concentration during entire measurement period at each site.
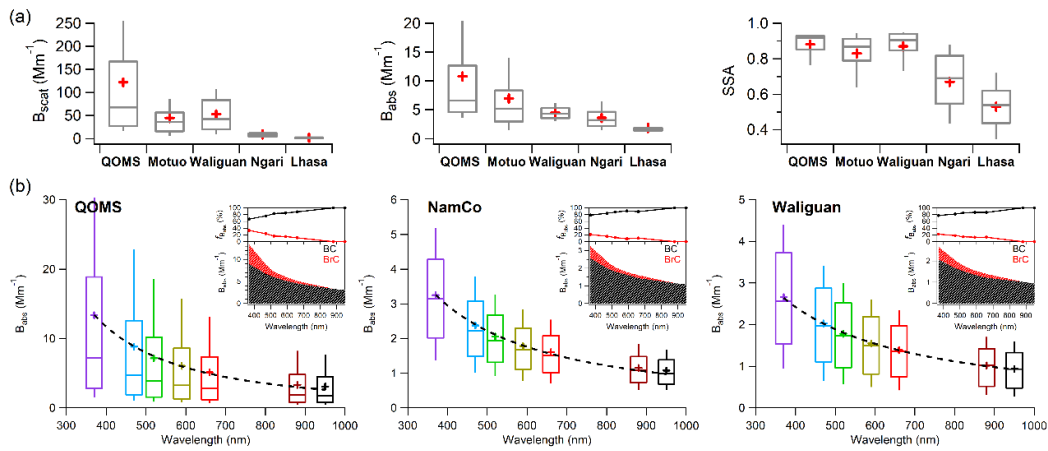
1468

Figure 8. Box plots of **(a)** the average particle light scattering coefficient (B_{scat}), light absorption coefficient (B_{abs}), and single scattering albedo (SSA) during the five aerosol field measurement campaigns at QOMS, Motuo, Waliguan, Ngari, and Lhasa sites, and **(b)** the particle B_{abs} at seven wavelengths measured by aethalometers at QOMS, NamCo, and Waliguan sites. The dashed lines in the boxes in **(b)** show the power-law fit of the average B_{abs} as a function of wavelength. The inserted plots in **(b)** are the apportioned contributions of BC and BrC to total B_{abs} at different wavelengths.
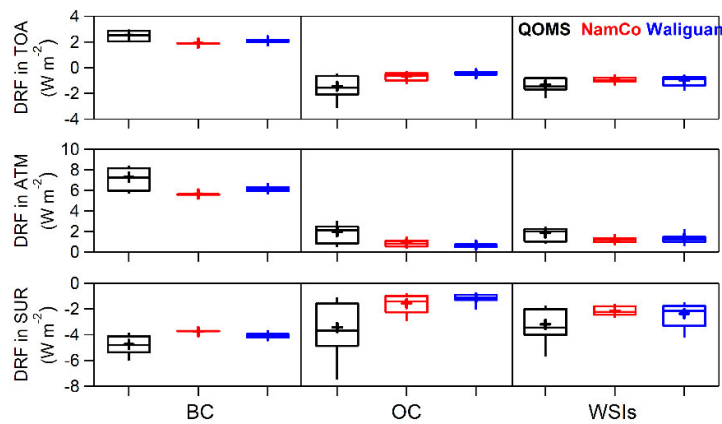
1476

Figure 9. Box-plots of the modelled direct radiative forcing (DRF) at the top of the atmosphere (TOA), the atmosphere (ATM), and the earth's surface (SUR) caused by black carbon (BC), organic carbon (OC), and water-soluble io ns (WSIs) during the QOMS, NamCo, and Waliguan campaigns.
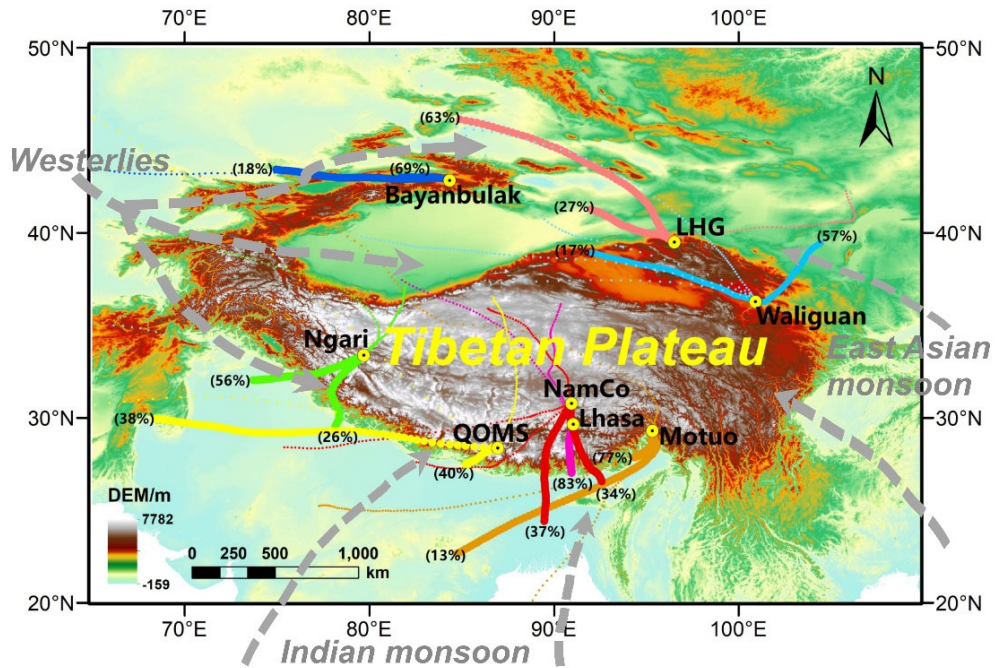
1480

Figure 10. ~~The average~~Average air mass backward trajectory clusters during the eight field campaigns in the Tibetan Plateau and its surroundings in our study (The geographical base map is created with ArcGIS). The major trajectory clusters ~~belong~~belonging to each field campaign are displayed using the relatively large solid circles in different colors with contributions marked ~~in the corresponding brackets~~, while the rest clusters with less contributions are exhibited in small dots.

Tables

Table 1. Detailed information about the full name and geographic characteristic of observation station, sample period, online instruments, and corresponding references during each aerosol field measurement campaigns over the Tibetan Plateau and its surroundings in this study.

Station	Full Station Name	Lat. (°N)	Long. (°E)	Alt. (m)	Sample Period	Online Instruments						References
						HR-ToF-AMS		SMPS	PAX	Aethal ometer	CCN -100	
						MS	PToF					
QOMS	Qomolangma Station for Atmospheric and Environmental Observation and Research, Chinese Academy of Sciences	28.36	86.95	4276	12 April to 12 May 2016	√	√	√	√	√		Zhang et al. (2018) An et al. (2019) Xu et al. (2020) Zhang et al. (2021) Xu et al. (2022)
Motuo	Motuo County, Linzhi City, Tibet Autonomous Region, China	29.30	95.32	1305	26 Mar to 22 May 2021	√	√	√	√		√	This study
NamCo	Nam Co Station for Multisphere Observation and Research, Chinese Academy of Sciences	30.77	90.95	4730	31 May to 1 July 2015	√				√		Xu et al. (2018) Zhang et al. (2021)
Ngari	Ngari Station for Desert Environment Observation and Research, Chinese Academy of Sciences	33.39	79.70	4270	1 Jun to 5 Jul 2022	√	√		√			This study
Waliguan	China Global Atmospheric Watch Baseline Observatory, Mount Waliguan Base	36.28	100.90	3816	1 July to 31 July 2017	√	√		√	√	√	Zhang et al. (2019) Zhang et al. (2020) Xu et al. (2020) Zhang et al. (2021) Xu et al. (2022)
LHG	Qilian Observation and Research Station of Cryosphere and Ecologic Environment, Chinese Academy of Sciences	39.50	96.51	4180	4 August to 29 August 2020	√		√			√	This study
Bayanbulak	Bayanbulak Town, Hejing County, Bayingolin Mongolian Autonomous Prefecture, Xinjiang Uygur Autonomous Region, China	42.83	84.35	2454	29 August to 26 September 2021	√	√					This study
Lhasa	Lhasa City, Tibet Autonomous Region, China	29.65	91.03	3650	31 August to 26 September 2019	√	√	√	√			Zhao et al. (2022)

1490

Table 2. Summary of the average values measured with various instruments during the eight aerosol field measurement campaigns in the TP and its surroundings in this study.

Measurement items	QOMS	Motuo	NamCo	Ngari	Waliguan	LHG	Bayanbulak	Lhasa
HR-ToF-AMS measurements								
PM$_1$ mass conc. (μg m^{-3})	4.4	5.7	2.0	4.1	9.1	3.0	1.9[a]	4.7
PM$_1$ chemical compositions (%)								
OA	54.4	57.0	68.0	56.3	34.5	23.1	38.4	82.6
Sulfate	9.3	21.1	15.0	19.8	38.1	46.0	41.6	3.4
Nitrate	5.1	2.3	2.0	5.7	8.1	5.7	5.4	5.4
Ammonium	5.8	7.3	7.0	9.2	15.2	14.4	13.6	4.7
Chloride	0.4	0.2	0	0.4	1.1	1.2	1.0	0.7
BC	25.0	12.1	8.0	8.6	3.0	9.7	N/A	3.1
Peak diameter in mass size distribution (nm)								
OA	510.2	430.5		584.4	405.5		350.8	228.1
SNA	510.2	471.9		634.5	504.7		379.6	250.0
OA components (%)								
MO-OOA	42.2	36.9	59.0	43.7	34.4	24.9	66.3	
LO-OOA		46.9	41.0	28.5		75.1	33.7	
OOA								34.0
BBOA	3.9	16.2		27.8	18.3			13.8
agBBOA					40.4			
NOA	13.9							
HOA						6.9		16.9
COA								35.3
OA elemental ratios								
O/C	1.19	0.99	1.07	0.98	0.99	1.14	0.69	0.44
H/C	1.29	1.55	1.48	1.33	1.41	1.05	1.52	1.76
OM/OC	2.70	2.48	2.57	2.44	2.45	2.62	2.09	1.74
N/C	0.030	0.020	0.016	0.019	0.008	0.011	0.026	0.001
SMPS measurements								
Number conc. (cm^{-3})	709.3	1639.2				1462.0		3994.4
Peak diameter in PNSD (nm)	109.4	131.0				42.9		28.9
PAX measurements								
B_{scat} (Mm^{-1})	121.9	44.9		8.9	36.3			2.1
B_{abs} (Mm^{-1})	10.8	7.0		3.6	4.1			1.9
B_{ext} (Mm^{-1})	132.7	51.9		12.6	40.4			4.0
SSA	0.89	0.83		0.67	0.86			0.52
Aethalometer measurements								
$B_{abs,370}$ (Mm^{-1})	13.40		3.25		2.66			
Absorption Ångström exponent	1.73		1.28		1.12			
$B_{abs,BrC,370}$ (Mm^{-1})	4.42		0.69		0.60			
$B_{abs,BC,370}$ (Mm^{-1})	8.94		2.56		2.06			
$fB_{abs,BrC,370}$ (%)	33.1		21.3		22.4			
$fB_{abs,BC,370}$ (%)	66.9		78.7		77.6			
CCN-100 measurements (cm^{-3})								
CCN number conc. (*SS* 0.2%)		974.0			~~507.0~~233.7	~~83.9~~120.5		
CCN number conc. (*SS* 0.4%)		1142.6			~~805.1~~857.8	~~344.3~~340.1		
CCN number conc. (*SS* 0.6%)		1240.1			~~1073.3~~1138.7	~~429.9~~417.8		
CCN number conc. (*SS* 0.8%)		1296.5			~~1230.6~~1313.1	~~480.8~~468.0		
CCN number conc. (*SS* 1.0%)		1337.9			~~1336.6~~1407.0	~~516.1~~504.5		

1493   [a]only non-refractory PM$_1$ is reported at Bayanbulak due to the absence of BC observation.

1494 **Table 3.** Summary of the average PM$_1$ mass concentrations (µg m^{-3}) measured by the Aerodyne
1495 AMSs at various high-altitude and remote sites worldwide.

Observation Sites	Latitude (°N)	Longitude (°E)	Altitude (m a.s.l.)	PM$_1$ mass (µg m^{-3})	References
QOMS, China	28.36	86.95	4276	4.4	This study & Zhang et al. (2018)
Motuo, China	29.30	95.32	1305	5.7	This study
NamCo, China	30.77	90.95	4730	2.0	This study & Xu et al. (2018)
Ngari, China	33.39	79.70	4270	4.1	This study
Waliguan, China	36.28	100.90	3816	9.1	This study & Zhang et al. (2019)
LHG, China	39.50	96.51	4180	3.0	This study
Bayanbulak, China	42.83	84.35	2454	1.9[a]	This study
Lhasa, China	29.65	91.03	3650	4.7	This study & Zhao et al. (2022)
NamCo, China	30.77	90.95	4730	1.06	Wang et al. (2017)
Mt. Yulong, China	27.20	100.20	3410	5.7	Zheng et al. (2017)
Menyuan, China	37.61	101.26	3295	11.4	Du et al. (2015)
Mt. Wuzhi, China	18.84	109.49	958	10.9	Zhu et al. (2016)
Mt. Jungfraujoch, Switzerland	46.55	7.98	3580	0.55	Fröhlich et al. (2015)
Mt. Jungfraujoch, Switzerland	46.55	7.98	3580	2.24	Zhang et al. (2007a)
Mt. Bachelor, USA	43.98	-121.69	2800	15.10	Zhou et al. (2017)
Mt. Whistler, Canada	50.01	-122.95	2182	1.91	Sun et al. (2009)
Mt. Cimone, Italy	44.18	10.70	2165	4.5	Rinaldi et al. (2015)
Puy de Dôme, France	45.77	2.95	1465	5.58	Freney et al. (2011)
Sub-Antarctic Bird Island	-54.00	-38.04		0.46	Schmale et al. (2013)
Mace Head, Ireland	53.30	-9.80		1.53	Zhang et al. (2007a)
Hyytiala, Finland	61.90	24.30		2.04	Zhang et al. (2007a)
Storm Peak, USA	40.50	-106.70		2.11	Zhang et al. (2007a)
Duke Forest, USA	36.00	-79.10		2.82	Zhang et al. (2007a)
Chebogue, Canada	43.80	-66.10		2.91	Zhang et al. (2007a)
Okinawa Island, Japan	26.87	33.51		7.89	Jimenez et al. (2009)
Fukue Island, Japan	32.69	128.84		12.03	Takami et al. (2005)
Cheju Island, Korea	33.51	126.50		10.66	Jimenez et al. (2009)

1496 [a]only non-refractory PM$_1$ is reported at Bayanbulak due to the absence of BC observation.